doi:10.1038/nature10351

Methods

Sample acquisition

Lymphoma samples were classified by an expert haematopathologist (R.D.G) according to the World Health Organization criteria of 2008. Benign specimens included reactive pediatric tonsils or purified CD77-positive centroblasts sorted from reactive tonsils using Miltenyi magnetic beads (Miltenyi Biotec, CA). The tumour specimens were collected as part of a research project approved by the University of British Columbia-British Columbia Cancer Agency Research Ethics Board (BCCA REB) and are in accordance with the Declaration of Helsinki. Informed consent was obtained from all individuals whose samples were profiled using RNA-seq or genome/exome sequencing. Our protocols stipulate that these data will not be released into the public domain but can be made available via a tiered-access mechanism to named investigators of institutions agreeing by a materials transfer agreement that they will honour the same ethical and privacy principles required by the BCCA REB.

For all DLBCL samples profiled by RNA-seq, genome or exome sequencing in this study, tumour content was greater than 50% as assessed by: a) immunophenotyping using flow cytometry to detect the level of coexpression of CD19 and light chain restriction; or b) a pathologist review of an H&E-stained frozen section taken adjacent to the tissue that was cut and used for nucleic acid extraction. All other specimens used in this study were obtained at the time of diagnosis and were derived from archived fresh-frozen tissue or frozen tumour

cell suspensions. Constitutional DNA was obtained from peripheral blood or from B cell-negative sorted tumour cell suspensions (fraction eluted from cells captured by B Cell Isolation Kit II or CD19 MicroBeads (Miltenyi Biotec, CA)).

Cell lines

DB[51], DOHH-2[52], Karpas422[53], NU-DHL-1[54], NU-DUL-1[55], SU-DHL-6 and WSU-DLCL2[56] are cell lines obtained from DSMZ. Pfeiffer and Toledo were obtained from ATCC and all OCI-Ly[57] lines (1, 3, 7, 10 and 19) were obtained from Louis Staudt (US National Institutes of Health). The cell lines MD903, SU-DHL-9 and RIVA were obtained from Martin Dyer (University of Leicester, UK).

Preparation and sequencing of RNA-seq, genome and exon capture Illumina libraries

Genomic DNA for construction of genome and exome libraries was prepared from biopsy materials using the Qiagen AllPrep DNA/RNA Mini Kit (Qiagen). DNA quality was assessed by spectrophotometry (260 nm/280 nm and 260 nm/230 nm absorption ratios) and gel electrophoresis before library construction. DNA was sheared for 10 minutes using a Sonic Dismembrator 550 with a power setting of “7” in pulses of 30 seconds interspersed with 30 seconds of cooling (Cup Horn, Fisher Scientific) and then analysed on 8% PAGE gels. The 200 to 300bp DNA size fraction was excised and eluted from the gel slice overnight at 4 °C in 300 µL of elution buffer (5:1 (vol/vol) LoTE buffer (3 mM Tris-HCl, pH 7.5,

0.2 mM EDTA)/7.5 M ammonium acetate) and was purified using a Spin-X Filter Tube (Fisher Scientific) and ethanol precipitation. Genome libraries were prepared using a modified paired-end protocol supplied by Illumina Inc. This involved DNA end-repair and formation of 3′ adenosine overhangs using the Klenow fragment of DNA polymerase I (3′–5′ exonuclease minus) and ligation to Illumina PE adapters (with 5′ overhangs). Adapter-ligated products were purified on QIAquick spin columns (Qiagen) and PCR-amplified using Phusion DNA polymerase (NEB) and ten cycles with the PE primer 1.0 and 2.0 (Illumina). PCR products of the desired size range were purified from adapter ligation artifacts using 8% PAGE gels. DNA quality was assessed and quantified using an Agilent DNA 1000 series II assay (Agilent) and Nanodrop 7500 spectrophotometer (Nanodrop), and DNA was subsequently diluted to 10 nM. The final concentration was confirmed using a Quant-iT dsDNA HS assay kit and Qubit fluorometer (Invitrogen).

For genomic DNA sequencing, clusters were generated on the Illumina cluster stations using v1 cluster reagents. Paired-end reads were generated using v3 sequencing reagents on the Illumina GA_{iix} platform following the manufacturer's instructions. Image analysis, base-calling and error calibration were performed using v1.0 of Illumina's Genome analysis pipeline. The DLBCL genomes were sequenced with 100 nucleotide paired-end reads using the HiSeq2000 platform.

For RNA-seq analysis, we used a modified method similar to the protocol we have previously described[13]. Briefly, RNA was extracted from 15 x 20 μm sections cut from fresh-frozen lymph node biopsies using the MACS mRNA

isolation kit (Miltenyi Biotec), from 5–10 μg of DNase I–treated total RNA as per the manufacturer's instructions. Double-stranded cDNA was synthesized from the purified poly(A)$^+$ RNA using the Superscript Double-Stranded cDNA Synthesis kit (Invitrogen) and random hexamer primers (Invitrogen) at a concentration of 5 μM. The cDNA was fragmented by sonication and a paired-end sequencing library prepared following the Illumina paired-end library preparation protocol (Illumina). For exome sequencing, genomic DNA was extracted following the protocol supplied in the Qiagen AllPrep DNA/RNA Mini Kit (Cat#80204), and quantified using a Quant-iT dsDNA HS assay kit and a Qubit fluorometer (Invitrogen). Approximately 500ng DNA was sheared for 75 seconds at duty cycle “20%” and intensity of “5” using a Covaris E210, and run on an 8% PAGE gel. A 200 to 250bp DNA size fraction was excised and eluted from the gel slice, and was ligated to Illumina paired-end adapters following a standard protocol as previously described[13]. The adapter ligated DNA was amplified for 10 cycles using the PE primer set (Illumina) and purified as a pre-exome capture library. The DNA was assessed using an Agilent DNA 1000 Series II assay, and 500ng DNA was hybridized to the 38Mb Human exon probe using the All Exon Kit (Cat#G3362) following the Agilent SureSelect Paired-End Target Enrichment System Protocol (Version 1.0, September 2009). The captured DNA was purified using a Qiagen MinElute column, and amplified for 12 cycles using PE primer set. The PCR products were run on an 8% PAGE gel, the desired size range (320 to 370bp) was excised and purified, and was then assessed using an Agilent DNA 1000 series II assay and diluted to 10nM. The final library DNA

concentration was confirmed using a Quant-iT dsDNA HS assay kit and Qubit fluorometer. Clusters were generated on the Illumina cluster station and paired-end reads generated using an Illumina Genome Analyzer (GA_{IIx}) following the manufacturer's instructions.

Alignment-based analysis of tumour DNA and RNA sequence for somatic point mutations

All reads were aligned to the human reference genome (hg18) or (for RNA-seq) to a genome file that was augmented with a set of all exon-exon junction sequences using BWA version 0.5.4[46]. RNA-seq libraries were aligned with an in-house modified version of BWA that is aware of exon junction reads and considers them when determining pairing distance in the "sampe" (read pairing) phase of alignment. Candidate single-nucleotide variants (SNVs) were identified in the aligned genomic sequence reads and the transcriptome (RNA-seq) reads using an approach similar to one we previously described[13]. One key difference in our variant calling in this study was the application of a Bayesian SNV identification algorithm ('SNVmix')[47]. This approach is able to identify SNVs with a minimum coverage of two high-quality (Q20) bases. SNVs were retained if they had a SNVmix probability of at least 0.99 and had support from reads mapping to both genomic strands. Any SNV near gapped alignments or exactly overlapping sites assessed as being polymorphisms (SNPs) were disregarded, including variants matching a position in dbSNP or the sequenced personal genomes of Venter[58], Watson[59] or the anonymous Asian[60] and Yoruban[61] individuals. For

paired samples with matched constitutional DNA sequence, all variants with evidence (a SNVmix probability of at least 0.99 and 2 or more high quality base calls matching the SNV) in the constitutional DNA were considered germline variants and were no longer considered cSNVs. Mutations were annotated on genes using the Ensembl transcripts (version 54), except in the cases of *MEF2B* and *MLL2,* for which the Ensembl annotations were deemed inferior to the Refseq. Because we observed situations where exons were represented in Ensembl transcripts that were not also represented in a Refseq, we only report candidate mutations in exons shared by both annotations (e.g. in Supplementary Table S4). Candidate mutations were subsequently reviewed visually in the integrative genomics viewer (IGV)[62] and those appearing to be artefacts or with some evidence (2 or more reads) visible in the constitutional DNA sequence were removed.

Validation of candidate somatic mutations using Illumina sequencing

Validation was accomplished by designing primers to amplify a 200 to 300 bp region around the targeted variant with one primer within reach of a single read (i.e. maintaining the sum of the primer length and distance to variant less than 100bp, depending on read length used). Amplicons were generated for both tumour and normal DNA. Two pools of amplicons were generated, one for tumour and one for normal DNA, with equal volumes from each PCR reaction (or increased volume for amplicons that resulted in faint bands in an agarose gel) and an Illumina paired-end sequencing library was constructed from the pool.

For variants common to more than one patient, a 6nt index, which was added to the 5' end of each primer, was assigned for each patient. These index sequences were trimmed from sequence reads prior to alignment and subsequently used to associate the data with individual patients. Reads were aligned using BWA and variants were visually confirmed for validity and somatic status in IGV[63](absence from constitutional DNA). Variants with primer design or PCR failures were scored as 'unvalidated'.

Validation of cSNVs by Sanger sequencing

The majority of candidate cSNVs were validated by Sanger sequencing of the region surrounding each mutation. These included all cSNVs identified in the two DLBCL exomes and the FL genome/exome (i.e. DLBCL-PatientA, DLBCL-PatientB and FL-PatientA). For the additional DLBCL genomes, cSNVs were selected for validation only if there were three or more cSNVs in that gene in the entire cohort. To do so, primers were designed to amplify 350-1200bp regions by PCR (most amplicons were ~400bp). All primers used for mutation confirmation can be found in Supplementary Table S14. Forward and reverse primers were tailed with T7 and M13Reverse 5' priming sites, respectively. PCR conditions used were 94ºC for 2 minutes, 30 cycles of 94ºC for 30 seconds, 60ºC for 30 seconds and 72ºC for 1 minute, and a final extension at 72ºC for 8 minutes. To determine the somatic or germ line origin of the mutations, mutations were re-sequenced in both tumour and constitutional DNA, the latter obtained from peripheral blood or negative-sort cells (see section entitled Sample

Acquisition**)**. The sequencing reactions consisted of 50 cycles of 96ºC for 10 seconds, 43ºC (for M13Reverse) or 48ºC (T7) for 5 seconds and 60ºC for 4 minutes and were analysed using an AB 3730XL. All capillary traces were analysed using the Staden Package[64] and all somatic variants were visually inspected to confirm their presence in tumour and absence from germ line traces. Some regions that failed to amplify in the first attempt were re-addressed with the addition of 5% DMSO and 5% betaine to the sequencing reactions, but otherwise maintaining the PCR conditions. SNVs in certain genes, such as *BCL7A* and *HDAC7*, repeatedly failed to amplify and for these, it was not possible to address whether the mutations in these genes were somatically acquired or were present in the germ line. Validation was not performed for variants in *BCL2* or *CD79B* as their somatic mutation status in DLBCL is well established.

Detection of enrichment of functional gene classes within frequently mutated genes

Significant functional classes represented in the cSNV list were identified using the DAVID Functional Annotation tool (http://david.abcc.ncifcrf.gov/). Reported P values were corrected for multiple testing using the Benjamini method.

Detection of mutations with imbalanced/skewed expression

The analysis of imbalanced expression was restricted to (1) confirmed somatic nonsynonymous point mutations along with (2) previously published hot spot mutations. In total, there were 381 such mutations in 99 of the 109 genes

represented in the RNA-seq data. For each mutated gene, the number of aligned reads supporting the reference and mutant allele was determined. For genes with multiple mutations in the same patient (e.g. *BCL2*), the sum of all reads supporting each of the non-reference alleles in that patient was used instead (assuming that all mutations were restricted to the same allele). Significant imbalance/skew was computed using the binomial exact test and P values were corrected using the Bonferroni method. Genes with corrected P values less than 0.05 and skew in favour of the mutant allele are reported in Supplementary Table S7.

Calculation of selective pressure

To determine if mutational patterns were indicative of selective pressure, we considered both synonymous and non-synonymous cSNVs across our patient cohort (excluding those found to be present in the germ line or false positives after validation). Selection can be inferred when the type of mutations in a gene differs from those expected by chance given a specific mutation profile. To analyse the significance of this deviation we applied the methods described by Greenman and colleagues[20] to identify genes with signatures of selection. We performed this analysis on the 101 (of 109 total) genes that had, in addition to 2 or more confirmed somatic mutations, more than 2 cSNVs in total. The coding sequence of each gene (using the longest Refseq annotation for that gene) was scanned for all possible silent and non-silent mutations (missense and truncating) matching six types of sequence changes (C>A, C>G, C>T, T>A, T>C,

T>G). The separation of mutations into different strata allows the model to consider the overall effect that cancer specific mutation mechanisms may have on the mutation profile. A null-selection mutation profile is estimated via the synonymous mutations, under the assumption that they do not confer an advantage to the tumour. A score statistic describing the selective pressure was then calculated by comparing the expected mutations of each type to the observed ones. Statistical significance was then determined by constructing an empirical distribution of scores from 100,000 Monte Carlo simulations under the null hypothesis of no selection. The number of Monte Carlo iterations was increased to a maximum of 14,600,000 for genes that did not obtain a p-value at the default 100,000 simulations. Using the models described by Greenman *et al*[20] we also estimated the type and strength of the selective pressure the genes were under. This is represented by a quantitative value of less than, equal to, or larger than 1 for negative, null, or positive selection respectively (Table1, Supplementary Table S8).

Several genes in our list have previously been identified as targets of somatic hypermutation (SHM), which is mediated by the enzyme AICDA (also known as AID) and targets a limited number of genes in DLBCL[65,66]. In an attempt to avoid biasing the selective pressure model with the distinct mutational signature caused by somatic hypermutation, we split the genes into two sets. The hypermutation set contained genes previously reported to be targets of SHM (*BCL2*[17], *BCL6, IRF4, PIM1,* and *CIITA*) and the non-hypermutation set contained the remaining 95 genes. The effect of the different mutational profiles of both sets

can be appreciated by considering the *BCL2* case. When inserted into the model with the rest of the genes *BCL2* presented the highest selective pressure of all genes (65.65); however, when the selective pressure model was applied to the hypermutated genes separately, *BCL2* selective pressure was estimated at 3.78.

Identifying genes with mutation hot spots

Hot spots were identified by searching for clustered mutations in the cSNVs identified by RNA-seq. Owing to the lack of constitutional DNA sequence from some patient samples, we could not necessarily discern if the variants detected only by RNA-seq were present in the germ line. We specifically sought cases in which codons were recurrently mutated. To find hot spots in the RNA-seq data, we searched for sets of distinct variants producing non-synonymous changes affecting the same codon in different tumours. The genes that met this criterion (Supplementary Table S6) included known targets of recurrent mutation (*EZH2*, *CARD11*[18] and *CD79B*[9]) and three hot spots in *MEF2B*. Also among these genes were known targets of aberrant somatic hypermutation in DLBCL, including *BCL2*, *IRF4*[65], *PIM1*[66], *BCL6*[67], and *BCL7A*[65].

Analysis of aligned genomic DNA sequence for copy number alterations and LOH

For the identification of copy number variations (CNVs), sequence quality filtering was used to remove all reads of low mapping quality ($Q \leq 10$). Due to the varying numbers of sequence reads from each sample, aligned reference reads were

first used to define genomic bins of equal reference coverage to which depths of alignments of sequence from each of the tumour samples were compared. This resulted in a measurement of the relative number of aligned reads from the tumours and reference in bins of variable length along the genome, where bin width is inversely proportional to the number of mapped reference reads. After an estimate of differential GC bias was used to reduce noise, an HMM was used to classify and segment continuous regions of copy number loss, neutrality, or gain using methodology outlined previously[68].

Loss of heterozygosity was determined for each sample using the lists of genomic SNPs that were identified through the BWA / SNVMix pipeline. This analysis allows for classification of each SNP as either heterozygous or homozygous based on the reported SNP probabilities. For each sample, genomic bins of consistent SNP coverage were used by an HMM to identify genomic regions of consistent rates of heterozygosity. The HMM partitioned each tumour genome into three states: normal heterozygosity, increased homozygosity (low), and total homozygosity (high). We infer that a region of low homozygosity either represents a state where only a portion of the cellular population had lost a copy of a chromosomal region or the signal was convoluted due to contaminating normal cells in the tumour. Both states of reduced homozygosity are displayed in blue in Figure 1, generated by Circos[69].

Assembly-based analysis of tumour DNA and RNA sequence

Reads from the individual RNA-seq libraries were assembled using ABySS as previously described[70] using multiple values of k. Iterative pairwise alignments of the contigs from the individual kmer assemblies resulted in a merged contig set that was aligned against the reference Human genome (hg18) using BLAT as described[48]. Putative fusions were identified from contigs that had alignments to two distinct genomic locations. The putative events were filtered using evidence from alignment of reads to contigs using Bowtie and alignments of reads to the genome using BWA. Those events with at least four read pairs from the reads-to-genome alignment and two supporting reads from the reads-to-contig alignment (i.e. across the fusion breakpoint) were manually curated to produce a final list of putative fusions. The genomic breakpoints for the transcriptome predicted events were identified manually from the alignments of the reads to the genome using IGV. The genomic breakpoints were later confirmed by assembly using ABySS and these results are summarized in Supplementary Table S3.

Putative indels were identified from alignment of the contigs to hg18 using BLAT when contiguous unmatched base(s) were found in either the contig (insertion) or reference (deletion) sequences. The events were filtered for read support with events requiring three or more reads to be considered in the filtered set. The filtered set was then screened against dbSNP130 to find putative novel events. The resulting set was manually inspected using read alignments (against both the genome and contigs) to visually confirm candidates. This approach revealed the deletion in *GNA13* shown in Supplementary Figure S4.

The splicing alterations in *MLL2* (Figure 3B and C) and *GNA13* (Supplementary Figure S4) were identified from pairwise alignments of the contigs to hg18 using BLAT. The contig alignments were then matched against the four known gene models to identify novel splice junctions. The putative novel splice junctions were filtered where two or more reads were required across the novel junction for the event to be considered. Manual inspection using read alignments (against both the genome and contigs) was performed to visually confirm candidates.

Cell of origin subtype assignment using RNA-seq expression values

Global gene expression signatures measured with microarrays are the standard method for classifying DLBCL samples into the two molecular subtypes (GCB and ABC). We adapted the Bayesian method described by Wright et al[50] to allow classification to be accomplished with the expression values obtained from RNA-seq data. To accomplish this, expression values for each Ensembl gene model (version 54) were computed as FPKM (fragments per kilobase gene model per million, rather than RPKM to account for the use of paired-end reads) and log-transformed. The current standard approach for routinely classifying samples using Affymetrix U133 arrays employs 186 probesets (George Wright, personal communication). The 165 Ensembl genes that correspond to these probesets were used for classification by RNA-seq. The classifier was trained using the 43 cases previously classified as GCB and 21 classified as ABC using Affymetrix data. The FPKM values for these genes were compared between the samples

with known subtypes using the T test and those producing a P value < 0.01 were used for the classifier. The robustness of this approach was tested using leave-one-out cross-validation, which resulted in no mis-classifications. Similarly, no samples were mis-classified when all cases with known COO (based on Affymetrix data) were used to produce the classifier however there were some cases that were defined as unclassifiable (U) by one method and given a subtype assignment by the other method. In such cases, the subtype assignment (rather than U) was used and the discrepancies are noted in Supplementary Table S2.

Targeted *MEF2B* resequencing using Biotinylated RNA capture probes

The following strategy was used to sequence the entire *MEF2B* locus in multiple patient samples in multiplex. Four exonic regions of the *MEF2B* gene were amplified from a template consisting of a pool of DNAs from three bacterial artificial chromosomes (BACs) containing the *MEF2B* locus (M. Nefedov , P. J. de Jong and U Surtiby, unpublished) using PCR (Supplementary Table S14). PCR reactions consisting of 0.5 Units Phusion DNA Polymerase (New England Biolabs, Pickering, Ont.), 0.25 mM dNTPs, 3% DMSO, 0.4 µM of the forward and reverse primer and 5 pmol template were cycled on a MJR Pelletier Thermocycler (model PTC-225) for 30 seconds at 98^0C; 25 X {10 seconds at 98^0C, 30 seconds at 65^0C, 30 seconds at 72^0C}; 5 minutes at 72^0C. The resulting PCR amplicons, ranging in size from 342 to 474bp, were size selected on an 8% Novex-TBE gel (Invitrogen Canada Inc., Burlington, Ont.), excised and eluted into 300 µL of elution buffer containing 5:1 (vol/vol) LoTe (3mM Tris-HCl,

pH7.5, 0.2nM EDTA)/7.5 M ammonium acetate. The eluates were purified from gel slurries by centrifugation through Spin-X centrifuge tube filters (Fisher Scientific Ltd., Nepean, Ont.), and EtOH precipitated. Purified amplicon DNAs were quantified using an Agilent DNA 1000 Series II assay (Agilent Technologies Canada Inc., Mississauga, Ont.). Individual amplicons were pooled (equimolar) and sheared using the Covaris S2 focused ultra-sonicator (Covaris Inc., Woburn, Mass.) with the following settings; 10% Duty cycle, 5% Intensity, and 200 Cycles per burst for 180 seconds. The resulting products were size fractioned on an 8% Novex TBE gel (Invitrogen Canada Inc.) and the 75 to 125 bp fraction isolated, purified and quantified as above. 30 ng of resulting DNA was end-repaired, 3-prime modified with Adenosine overhangs, and ligated to custom adapters (Supplemental Table S14) containing T7 and T3 promoter sequences as described[71]. Adapter-ligated products were enriched by PCR as above using T3 and T7 sense strand-specific primers and the following cycling conditions; 1 min. at 98^0C; 8X {10 seconds at 98^0C, 30 seconds at 60^0C, 30 seconds at 72^0C}; 5 minutes at 72^0C. The amplified products were separated from excess adapter on an 8% Novex TBE gel (Invitrogen Canada Inc.), purified, and quantified using the Qubit Quant-iT™ assay and Qubit Fluorometer (Invitrogen Canada Inc.). An *in vitro* transcription reaction was carried out using 100 ng of purified adapter-ligated DNA as per the manufacturer's specifications (Ampliscribe™ T7-Flash™ Biotin-RNA Transcription Kit; Intersciences Inc., Markham, Ont.). The reaction mixture was incubated at 37^OC for 60 minutes, DNase-I treated for 15 minutes at 37^OC, and then incubated at 70 ^{O}C for 5 minutes to inactivate DNaseI.

Transcription products were precipitated with 1 volume of 5M NH_4Ac, and size fractioned on a 10% Novex TBE-Urea gel (Invitrogen Canada Inc.). The 100 to 150 bp fraction was isolated from the gel, eluted into 0.3M NaCl, and EtOH-precipitated after extraction of the eluate from the gel slurry by centrifugation through a Spin-X Filter centrifuge tube filter (Fisher Scientific Ltd.). The biotinylated RNA was resuspended in 20 µl nuclease-free water and quantified using an Agilent RNA Nano assay (Agilent Technologies Canada Inc.).

Indexed libraries of patient genomic DNA were pooled from 96 well plates in groups ranging from 36 to 47 libraries per pool[72]. A 250 to 350bp size fraction from each pool was size-selected by gel purification from an 8% Novex TBE gel as above (Invitrogen Canada Inc.). The protocol described by Gnirke and colleagues[73] was followed for the hybridization reaction and subsequent washes, with an additional oligonucleotide block consisting of standard Illumina PCR primers PE1 and PE2 included in the hybridization reaction mixture to prevent cross-hybridization between library fragments (Supplementary Table S14). The incubation of the library fragments with the RNA probe pool was carried out for 24 hours at 65^0C, followed by binding to M-280 Streptavidin Dynabeads (Invitrogen Canada Inc.), washes, and elution of the captured library fragments. The eluted fragments were amplified by PCR using primers that anneal upstream of the adapter index sites (Supplemental Table S14) and subjected to cluster generation and sequencing as described above.

Targeted *MLL2* resequencing using long-range PCR and sample indexing.

Due to the presence of inactivating mutations in different positions within the *MLL2* gene, we sequenced the entire *MLL2* locus (chr12:47,699,025-47,735,374; hg18) in a cohort of 35 FL and 37 DLBCL primary tumours, in 17 DLBCL derived cell lines and, as a control, in 8 centroblast samples. Genomic DNA from individual samples was normalized to 5 ng/µl, and 12.5 ng of each sample was PCR amplified using LA Taq DNA polymerase (TaKaRa). Twelve long amplicons, of sizes ranging from 6600bp to 7800bp, were obtained under the following PCR conditions: 94ºC for 5 minutes, 35 cycles of 98ºC for 10 seconds and 68ºC for 8 minutes, and a final extension at 72ºC for 10 minutes. The primer sets used are displayed in Supplementary Table S14. Amplicons were cleaned using AMPure beads (Beckman Coulter) and eluted with 20-µL of TE. All 12 amplicons per sample were normalized and pooled together.

An individual indexed library was constructed from each sample (comprising the pool of the 12 long amplicons from *MLL2*). Approximately 500 ng of each pooled DNA sample was sheared for 10 min using a Sonic Dismembrator 550 with a power setting of “7” in pulses of 30 seconds interspersed with 30 seconds of cooling (Cup Horn, Fisher Scientific) and then analysed on 8% PAGE gels. The 200 to 300bp DNA fraction was excised and eluted from the gel slice overnight at 4°C in 300 µL of elution buffer (5:1 (vol/vol) LoTE buffer (3 mM Tris-HCl, pH 7.5, 0.2 mM EDTA)/7.5 M ammonium acetate) and was purified using a Spin-X Filter Tube (Fisher Scientific) and by ethanol precipitation. Indexed libraries were prepared using a modified paired-end protocol. This involved DNA end-repair reactions at room temperature 20–25 °C for 30 minutes (5 U T4 DNA

polymerase, 1 U Klenow DNA polymerase (exonuclease minus), 100 U T4 polynucleotide kinase and 0.4 mM dNTP mix (Invitrogen). End-repair reactions were purified using AMPure beads, and dATP was added to the 3′ ends using 5 U Klenow DNA polymerase (exonuclease minus) and 0.2 mM dATP in 1× Klenow Buffer (Invitrogen) with 30-minute incubation at 37 °C in a Tetrad thermal cycler (MJ Research). DNA was again purified on AMPure beads using a Biomek FX. Adapter ligation (10:1 ratio) was completed with 0.03 μM adapter (multiplexing adapters 1 and 2), 100 ng DNA, 5 U T4 DNA ligase, 0.2 mM ATP and 1× T4 DNA Ligase Buffer (Invitrogen) for 30 minutes at room temperature. Adapter-ligated DNA was again purified using AMPure beads on a Biomek FX. A selection of DNA samples were quantified on a Qubit (Invitrogen). 15-cycle indexing enrichment PCR was performed using Phusion DNA polymerase and Primers 1.0 and 2.0 (IDT) and 96 custom indexing primers. PCR cycles were: 98°C for 60 seconds, followed by 15 cycles of 98°C for 10 seconds, 65°C for 15 seconds and 72°C for 30 seconds. The PCR products were purified using AMPure beads and eluted in 40 μL elution buffer EB (Qiagen). Product quality was assessed by quality-control gels with 1.75% SeaKem LE agarose in 1× TAE (0.2 μL of every amplicon) and on a 2100 Bioanalyzer (Agilent Technologies).

Indexed libraries were pooled together and sequenced on two lanes of a flowcell using an Illumina GA_{II} platform. Individual indexes allowed the deconvolution of reads deriving from individual samples in multiplexed libraries such that many cases were concurrently sequenced in the same flow cell lane. The reads were matched to patient samples using the index read and were aligned with BWA to

the human reference genome (hg18). Point mutations were identified using SNVMix with stringent post-filtration including a requirement for dual-strand coverage and requiring at least 10% of the aligned reads at a candidate variant to be non-reference. Insertions and deletions were identified using the SAMtools indel calling algorithm with similar filters. Only insertions and deletions supported by at least 2 reads on each strand were considered valid. The reported average coverage for each sample was calculated as the average depth of aligned reads across each of the coding (CDS) positions in the *MLL2* locus.

Re-confirmation of *MLL2* mutations in patient samples and DLBCL cell lines

MLL2 mutations found by targeted sequencing of *MLL2* in lymphoma samples were validated by Sanger sequencing of the region surrounding each mutation, except in 15 cases. To do so, primers were designed to amplify 400-600 bp regions by PCR. All primers used for mutation confirmation can be found in Supplementary Table S14. Validating forward and reverse primers carried T7 and M13Reverse 5' tails, respectively. PCR conditions used were 94ºC for 2 minutes, 30 cycles of 94ºC for 30 seconds, 60ºC for 30 seconds and 72ºC for 1 minute, and a final extension at 72ºC for 8 minutes. To determine the somatic or germline origin of the mutations, mutations were re-sequenced in both tumour and constitutional DNA, the latter obtained from peripheral blood or negative sort cells. The sequencing reactions consisted of 50 cycles of 96ºC for 10 sec, 43ºC

(for M13Reverse) or 48ºC (T7) for 5 seconds and 60ºC for 4 minutes and were analysed using an AB 3730XL. Variants were visually inspected to confirm their presence in tumour and absence from germline traces. In 8 of the patient samples that carried 2 mutations in *MLL2*, to establish whether one allele contained both mutations or each allele contained one, we sequenced both candidate mutations using DNA from BAC clones from FL patient libraries. The primers and PCR conditions were the same as those used for the validation of each of those mutations.

Targeted resequencing of *MEF2B* coding exons 1 and 2.

Coding exons 1 and 2 of *MEF2B* were PCR amplified using *MEF2B*_1F/R and *MEF2B*_2F/R primers (see Supplementary Table S14 for primer sequences) using the same conditions for *MLL2* (previous paragraph). Priming sites for T7 and M13Reverse were added to their 5′ ends to allow direct Sanger sequencing of amplicons. Amplicons were produced from whole genome amplified tumour genomic DNA from lymphoma patients and DLBCL cell lines. Whole genome amplification was performed using Repli-g Screening kit reagents (Qiagen), following the manufacturer instructions. All capillary traces were visually inspected.

Identification of structural aberrations involving *BCL2* and *BCL6*

The presence of translocations involving *MYC*, *BCL2* and *BCL6* was determined for 49 of the DLBCL cases (Supplementary Table S2; Figure 2) using commercial dual color “break-apart” probes from Abbott Molecular (Abbott Park, IL) on formalin fixed paraffin embedded tissue in tissue microarrays using the described method[74]. Additional fusion transcripts involving *BCL2* or *BCL6* were detected in these and the remaining libraries directly from the RNA-seq data using both Trans-ABySS[48] and deFuse (http://compbio.bccrc.ca/?page_id=275).

Analysis of impact of COO and mutation status on outcome in DLBCL

The analysis included only patients treated with curative intent who received at least one cycle of R-CHOP. Overall survival (OS) was calculated as the time from date of diagnosis until death from any cause. Patients were censored at the time they were last known to be alive. OS was assessed using the Kaplan-Meier method and the log rank test was used for comparison between groups. Data were analysed using SPSS software (SPSS version 14.0 for Windows; SPSS Inc, Chicago, IL).

References

51. Beckwith, M., Longo, D.L., O'Connell, C.D., Moratz, C.M. & Urba, W.J. Phorbol ester-induced, cell-cycle-specific, growth inhibition of human B-lymphoma cell lines. *J. Natl. Cancer Inst.* **82**, 501-509 (1990).
52. Kluin-Nelemans, H.C., Limpens, J., Meerabux, J., Beverstock, G.C., Jansen, J.H., et al. A new non-Hodgkin's B-cell line (DoHH2) with a chromosomal translocation t(14;18)(q32;q21). *Leukemia* **5**, 221-224 (1991).
53. Dyer, M.J., Fischer, P., Nacheva, E., Labastide, W. & Karpas, A. A new human B-cell non-Hodgkin's lymphoma cell line (Karpas 422) exhibiting both t (14;18) and t(4;11) chromosomal translocations. *Blood* **75**, 709-714 (1990).
54. Winter, J.N., Variakojis, D. & Epstein, A.L. Phenotypic analysis of established diffuse histiocytic lymphoma cell lines utilizing monoclonal antibodies and cytochemical techniques. *Blood* **63**, 140-146 (1984).
55. Epstein, A., Variakojis, D., Berger, C. & Hecht, B. Use of novel chemical supplements in the establishment of three human malignant lymphoma cell lines (NU-DHL-1, NUDUL-1, and NU-AMB-1) with chromosome 14 translocations. *International Journal of Cancer* **35**, 619-627 (1985).
56. Al-Katib, A.M., Smith, M.R., Kamanda, W.S., Pettit, G.R., Hamdan, M., et al. Bryostatin 1 down-regulates mdr1 and potentiates vincristine cytotoxicity in diffuse large cell lymphoma xenografts. *Clin Cancer Res* **4**, 1305-1314 (1998).
57. Mehra, S., Messner, H., Minden, M. & Chaganti, R.S.K. Molecular cytogenetic characterization of non-Hodgkin lymphoma cell lines. *Genes Chromosom. Cancer* **33**, 225-234 (2002).
58. Levy, S., Sutton, G., Ng, P., Feuk, L., Halpern, A., et al. The diploid genome sequence of an individual human. *PLoS Biol* **5**, e254-e254 (2007).
59. Wheeler, D.A., Srinivasan, M., Egholm, M., Shen, Y., Chen, L., et al. The complete genome of an individual by massively parallel DNA sequencing. *Nature* **452**, 872-876 (2008).
60. Wang, J., Wang, W., Li, R., Li, Y., Tian, G., et al. The diploid genome sequence of an Asian individual. *Nature* **456**, 60-65 (2008).
61. Bentley, D.R., Balasubramanian, S., Swerdlow, H.P., Smith, G.P., Milton, J., et al. Accurate whole human genome sequencing using reversible terminator chemistry. *Nature* **456**, 53-59 (2008).
62. Robinson, J.T., Thorvaldsdóttir, H., Winckler, W., Guttman, M., Lander, E.S., et al. Integrative genomics viewer. *Nat Biotechnol* **29**, 24-26 (2011).
63. Robinson, M.D. & Oshlack, A. A scaling normalization method for differential expression analysis of RNA-seq data. 1-9 (2010).
64. Staden, R. The Staden sequence analysis package. *Mol. Biotechnol.* **5**, 233-241 (1996).
65. Pasqualucci, L., Guglielmino, R., Malek, S.N., Novak, U., Compagno, M., et al. Aberrant Somatic Hypermutation Targets an Extensive Set of Genes in Diffuse Large B-Cell Lymphoma. *ASH Annual Meeting Abstracts* **104**,

1528-1528 (2004).
66. Pasqualucci, L., Neumeister, P., Goossens, T., Nanjangud, G., Chaganti, R., et al. Hypermutation of multiple proto-oncogenes in B-cell diffuse large-cell lymphomas. *Nature* **412**, 341-346 (2001).
67. Pasqualucci, L., Migliazza, A., Basso, K., Houldsworth, J., Chaganti, R.S.K., et al. Mutations of the BCL6 proto-oncogene disrupt its negative autoregulation in diffuse large B-cell lymphoma. *Blood* **101**, 2914-2923 (2003).
68. Jones, S.J., Laskin, J., Li, Y.Y., Griffith, O.L., An, J., et al. Evolution of an adenocarcinoma in response to selection by targeted kinase inhibitors. *Genome Biol* **11**, R82-R82 (2010).
69. Krzywinski, M., Schein, J., Birol, I., Connors, J., Gascoyne, R., et al. Circos: an information aesthetic for comparative genomics. *Genome Res* **19**, 1639-1645 (2009).
70. Birol, I., Jackman, S., Nielsen, C., Qian, J., Varhol, R., et al. De novo Transcriptome Assembly with ABySS. *Bioinformatics* (2009).doi:btp367 [pii] 10.1093/bioinformatics/btp367
71. Robertson, G., Hirst, M., Bainbridge, M., Bilenky, M., Zhao, Y., et al. Genome-wide profiles of STAT1 DNA association using chromatin immunoprecipitation and massively parallel sequencing. *Nat Meth* **4**, 651-657 (2007).
72. Wiegand, K.C., Shah, S.P., Al-Agha, O.M., Zhao, Y., Tse, K., et al. ARID1A mutations in endometriosis-associated ovarian carcinomas. *N Engl J Med* **363**, 1532-1543 (2010).
73. Gnirke, A., Melnikov, A., Maguire, J., Rogov, P., LeProust, E., et al. Solution hybrid selection with ultra-long oligonucleotides for massively parallel targeted sequencing. *Nat Biotechnol* **27**, 182-189 (2009).
74. Chin, S., Daigo, Y., Huang, H., Iyer, N.G., Callagy, G., et al. A simple and reliable pretreatment protocol facilitates fluorescent in situ hybridisation on tissue microarrays of paraffin wax embedded tumour samples. *MP, Mol. Pathol.* **56**, 275-279 (2003).

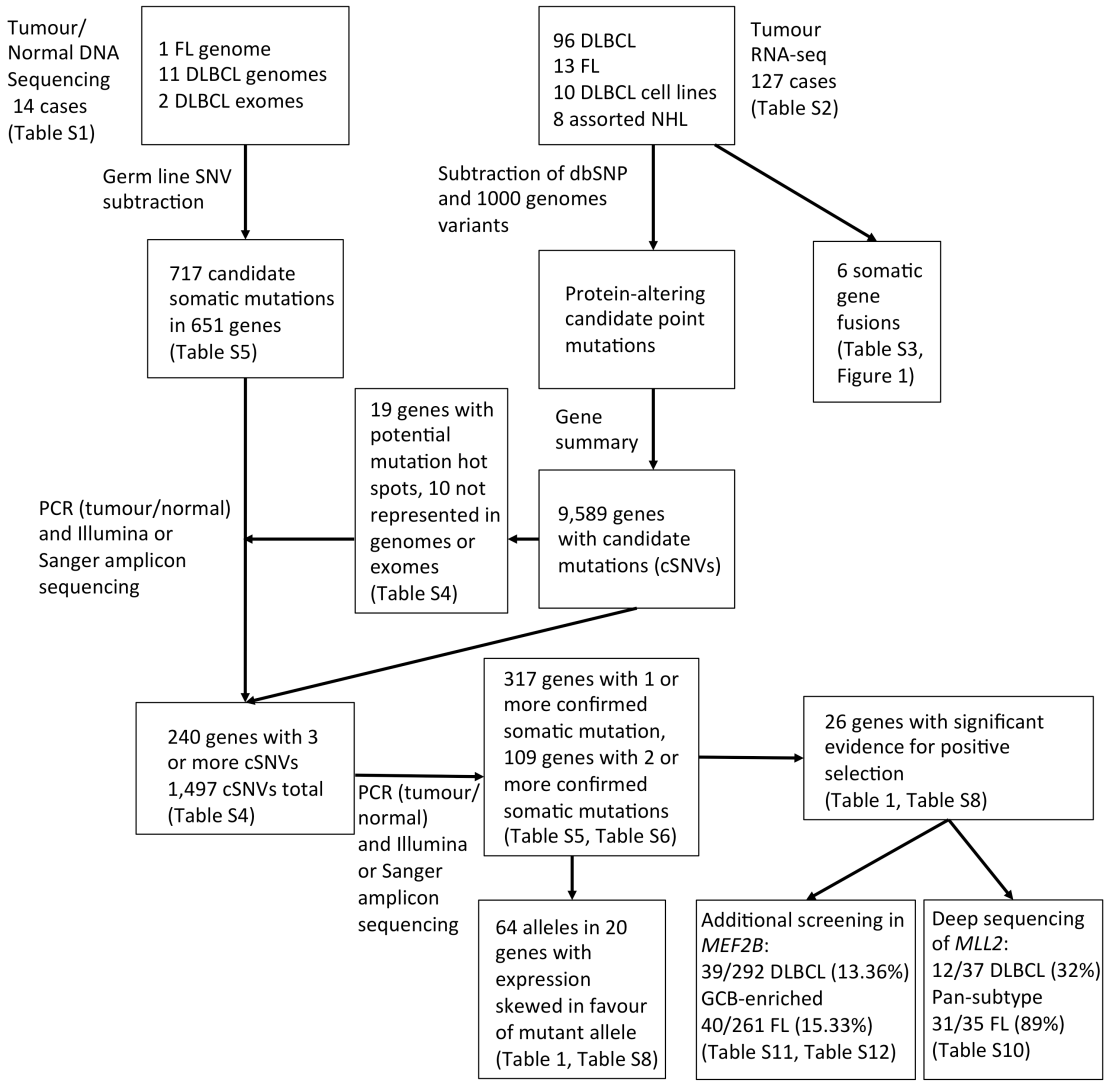

Figure S1: Overview of strategy. The samples analysed, experiments performed and an overview of the results. 717 nonsynonymous candidate somatic mutations in 651 genes were identified from the genomes/exomes of 14 NHL patient samples with matched constitutional DNA. Ten genes with hot spots were identified directly from the RNA-seq and nine of these genes were not among the 651 (661 total genes). We determined that 230 of these genes contained 3 or more cSNVs when genome and RNA-seq data were combined. We also attempted validation of all cSNVs identified in the FL genome and two DLBCL exomes. We validated at least one somatic cSNV in 317 genes (Table S5) and identified two or more somatic mutations in 109 genes using PCR amplification and Sanger sequencing in tumour and normal DNA. Of the successfully re-sequenced cSNVs predicted from the genomes, 171 (94.5%) were confirmed somatic, 7 were false calls and 3 were present in the germ line (Table S5). The entire *MLL2* locus was screened for additional mutations in 37 DLBCL and 35 FL samples. *MEF2B* was similarly sequenced in an extension cohort of 292 DLBCLs and 261 FLs.

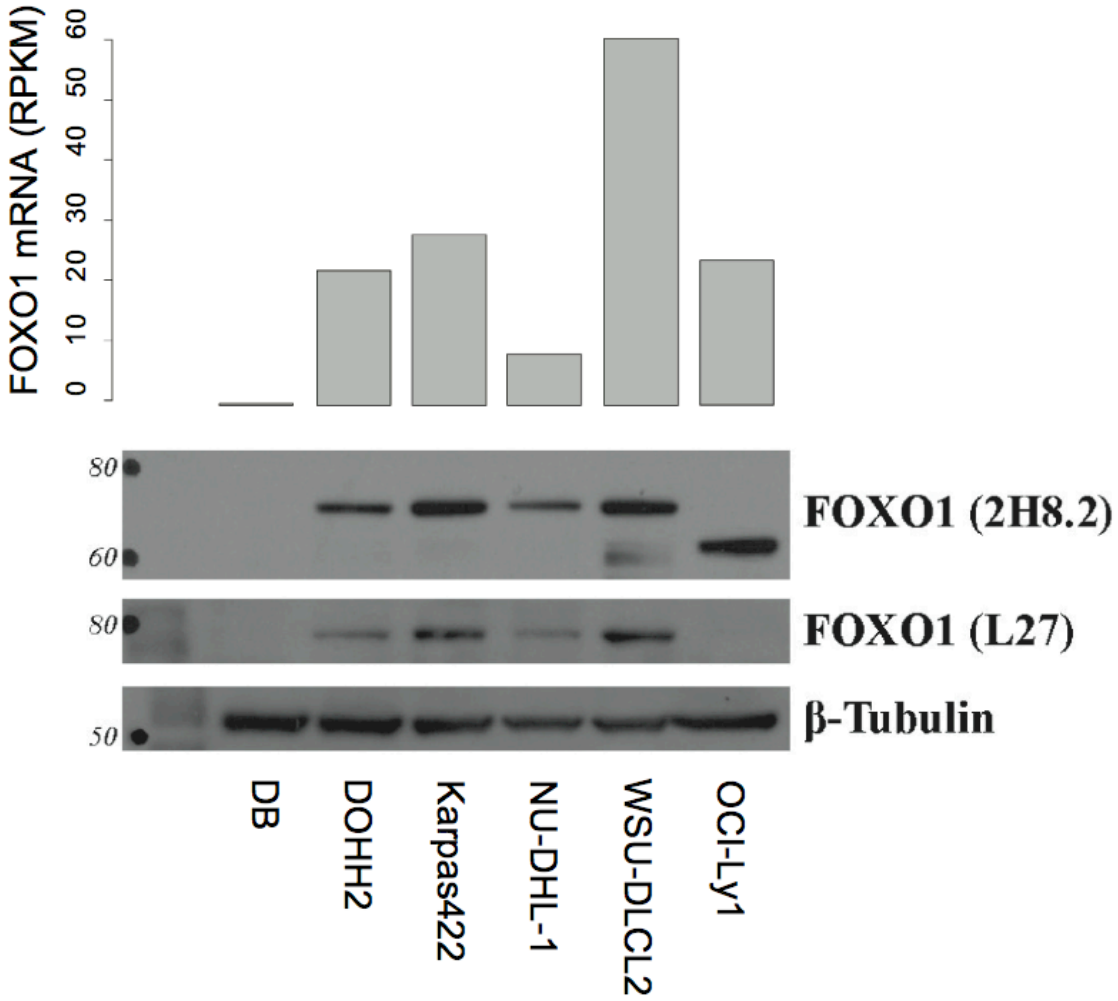

Figure S2: N-terminal truncation of FOXO1 protein with mutation affecting initial codon. (A) The RNA-seq data of cell lines and patient samples revealed mutations in 3 samples affecting the initial codon of *FOXO1*. To determine the effect of such mutations on FOXO1 protein, we assayed FOXO1 by Western blot in DLBCL cell lines using an antibody raised against full-length FOXO1 (2H8.2). In the cell line containing a mutation at the initiator methionine (OCI-Ly1), we observed a FOXO1 band of reduced molecular weight, compared to *FOXO1* wild-type cell lines (size indicated in Kilodaltons on the left). The reduced size is consistent with the use of a second methionine codon in the *FOXO1* gene, producing a protein shortened at the amino terminus by 70 amino acids. The same blot was also probed with an antibody that recognizes an N-terminal epitope (L27) and lack of a band in OCI-Ly1 cells is consistent with the notion that the lower band in this cell line corresponds to FOXO1 protein lacking its N-

terminus. We also noted absence of the protein in the DB cell line, which showed significantly reduced mRNA levels as measured by RNA-seq (upper bar chart; RPKM = Reads Per Kilobase of gene model per Million mapped reads).

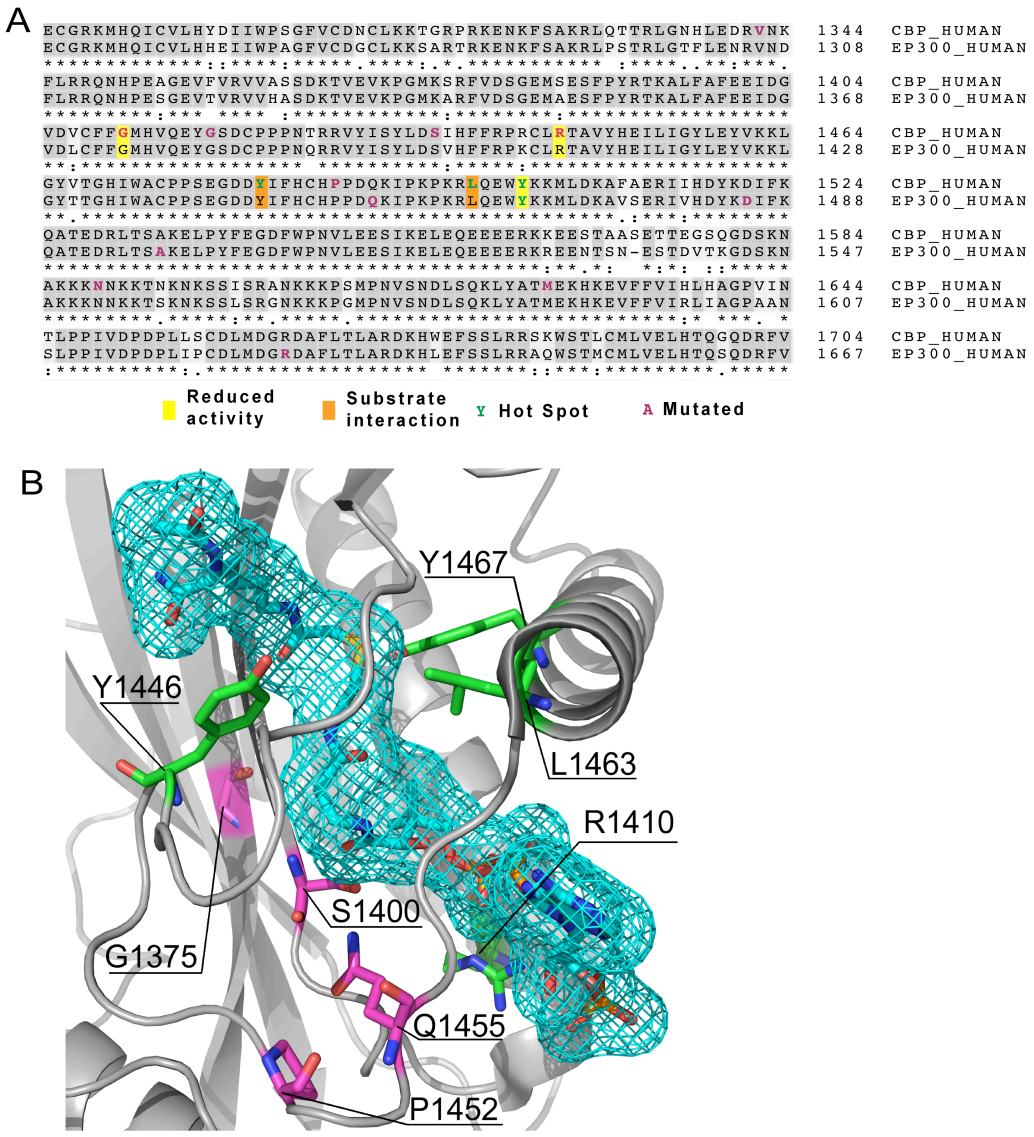

Figure S3: Recurrent mutations affecting the HAT domain of CREBBP and EP300.

Mutations affecting both *CREBBP* and *EP300* were detected. (A) Alignment shows the histone acetyltransferase (HAT) domain of both CREBBP and EP300 proteins. Residues with cSNVs in either CREBBP or EP300 are coloured pink if affected in a single sample or green if affected in multiple samples (i.e. hot spots). Yellow indicates that mutation of the highlighted residue has been shown to reduce HAT activity *in vitro* and orange indicates that the residue interacts with the substrate analogue utilized in solving the crystal structure (Lys-CoA)[1] (B) The three dimensional structure of the HAT domain of CREBBP and EP300 based on the solved structure of EP300[1]. Mutated residues in the HAT domain of both CREBBP and EP300 are highlighted with the same colouring as (A) with positions numbered relative to EP300. Many of the mutated residues are in close proximity to the substrate (shown here is the substrate analogue and inhibitor Lys-CoA, blue-caged molecule).

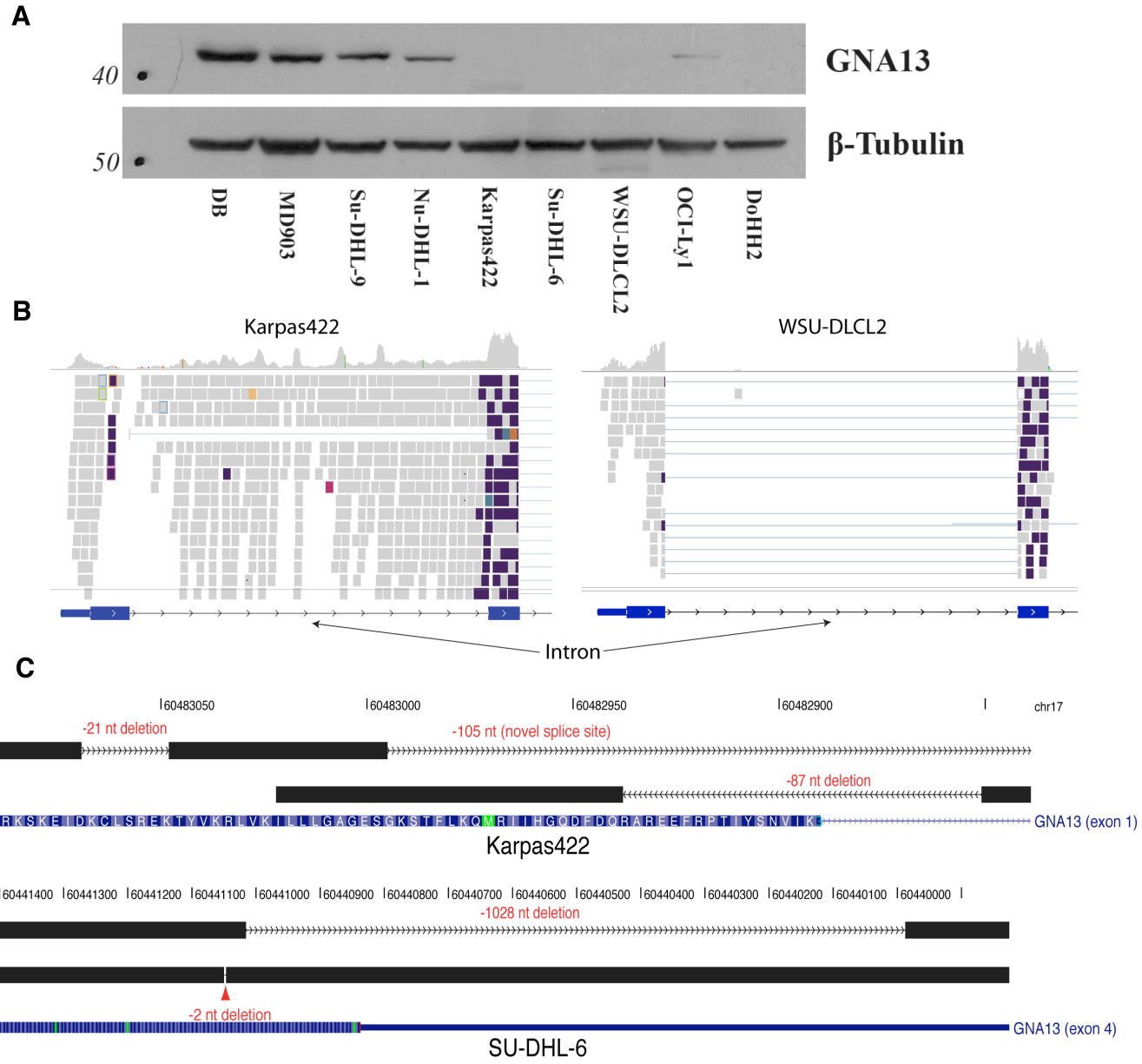

Figure S4: The effect of GNA13 mutations at the protein level.
(A) A western blot revealed the expected lack of GNA13 protein in DOHH2, the cell line with a truncating point mutation detected in the RNA-seq data. The lack of protein in Karpas422, SU-DHL-6 and WSU-DLCL2 was surprising, as we had not detected protein-truncating mutations in these cells. (B) Further analysis of the aligned sequence from these three cell lines and additional analysis utilizing a de-novo transcript assembly approach (Trans-ABySS; Methods), revealed multiple aberrations that may explain the lack of protein. Firstly, in Karpas422 reads were observed to map the first intron, suggesting that the intron is retained in a significant proportion of *GNA13* transcripts (compare Karpas422 on the left to WSU-DLCL2 on the right). Inspection of sequence contigs from this case

revealed the likely cause of intron reads to be a deletion of 87 nt that removes the canonical splicing donor from this exon (Panel C, top). Splicing still appears to occur to a lesser extent using a non-GT donor. Assembled reads from SU-DHL-6 revealed a 2 nt deletion and a large 1028 nt deletion. The former would affect the reading frame and the latter removes the terminal stop codon. Finally, in WSU-DLCL2, the splicing donor after the third exon was apparently mutated, converting the GT donor to a GC sequence (not shown). As in the Karpas422 case, there was clear evidence for retention of this intron in *GNA13* transcripts in WSU-DLCL2. Intron retention has previously been linked to nonsense-mediated transcript degradation[2] and if that is the case here, could explain the lack of GNA13 protein in these cells.

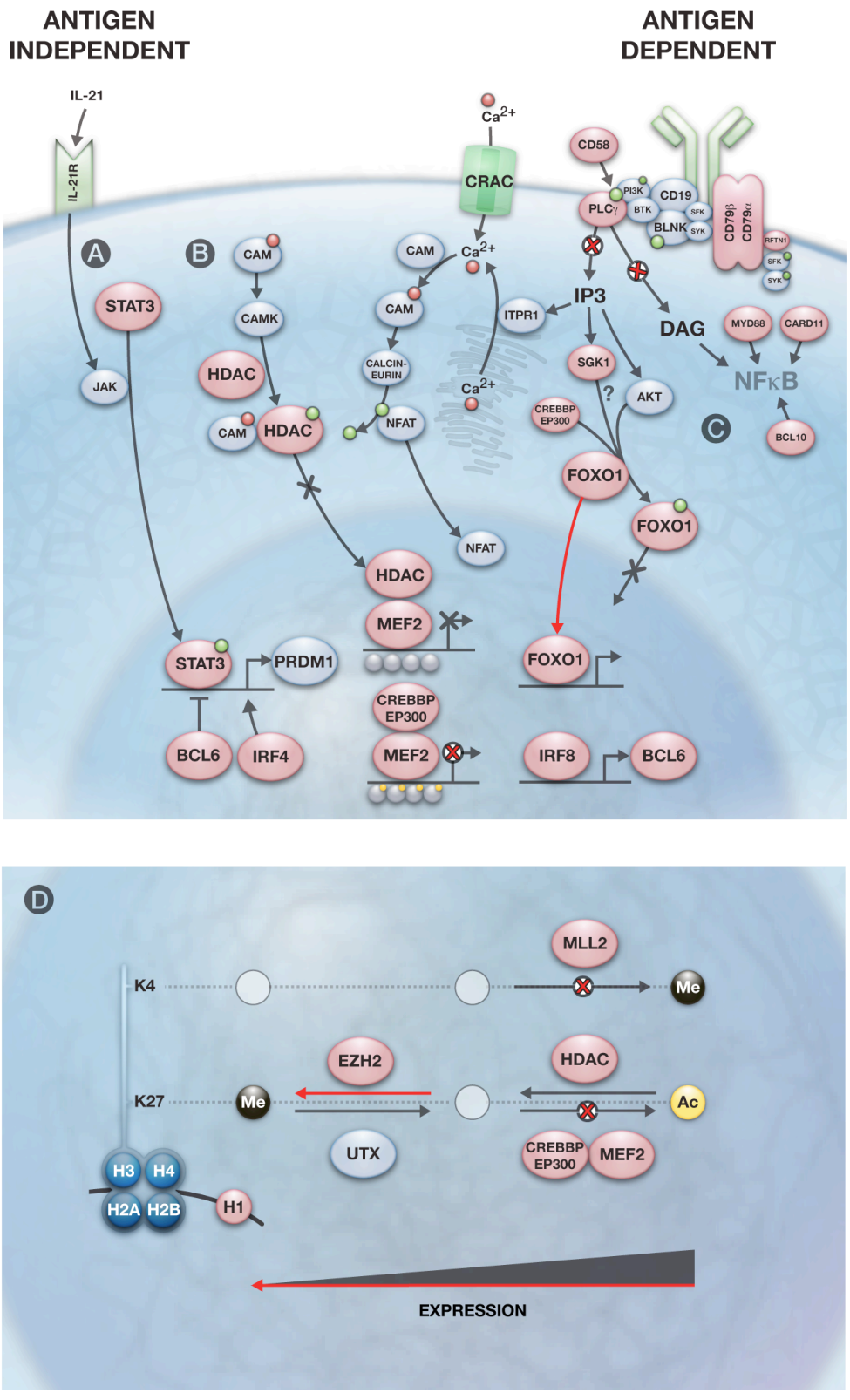
ANTIGEN INDEPENDENT
ANTIGEN DEPENDENT
IL-21
IL-21R
JAK
STAT3
A
B
CAM
CAMK
HDAC
CAM
HDAC
CAM
CALCIN-EURIN
NFAT
Ca2+
CRAC
Ca2+
CAM
Ca2+
ITPR1
IP3
DAG
CD58
PI3K
PLCγ
BTK
CD19
BLNK
SFK
SYK
CD79β
CD79α
RFTN1
SFK
SYK
MYD88
CARD11
NFκB
BCL10
C
SGK1
?
AKT
CREBBP EP300
FOXO1
FOXO1
NFAT
HDAC
MEF2
STAT3
PRDM1
BCL6
IRF4
CREBBP EP300
MEF2
FOXO1
IRF8
BCL6
D
MLL2
K4
Me
EZH2
HDAC
K27
Me
Ac
UTX
CREBBP EP300
MEF2
H3
H4
H2A
H2B
H1
EXPRESSION
repeatedly mutated gene
expected effect of mutation
phosphorylation
calcium

Figure S5: Potential impact of recurrently mutated genes on BCR signalling and downstream messengers.

(A) Autocrine and paracrine stimulation of IL-21R induces the dimerization and activation of STAT3, a positive regulator of *PRDM1* expression[3]. Mutations affecting the DNA binding domain of STAT3 are known to act as dominant negatives, which would predict the inability to induce *PRDM1* expression following IL-21 stimulation. (B) Multiple mutations predicted to directly alter BCR signalling or alter the normal events subsequent to BCR-induced influx of the secondary messenger Ca^{2+}. Cross-linking of CD58 has been shown to result in the phosphorylation of BLNK, Syk and PLC-gamma and lead to Akt activation[4]. Various mutations are expected to alter the ability of B cells to induce the expression of MEF2 target genes in response to the Ca^{2+} influx. The role of MEF2 gene family members in mediating epigenetic alterations downstream of the BCR has been inferred from a knockout study in which MEF2C was shown to be required for mediating calcium-dependent response to BCR signalling[5] and the involvement of CREBBP/EP300 in this process has been inferred from MEF2-mediated transcriptional regulation in other cell types including T cells[6]. This model predicts that influx of Ca^{2+} after BCR stimulation would result in the displacement of HATs by activated Calmodulin-dependent protein kinase (CAMK), allowing HDAC activity via CREBBP/EP300 thus enabling transcription at MEF2 target loci. In this model, mutation of any of these three genes and potentially the S155F mutation in *HDAC7* would diminish this effect and suppress the induction of MEF2 target loci after BCR stimulation. (C) Multiple mutations may affect the regulation of the activity of FOXO proteins following BCR stimulation. FOXO1 is a downstream target of the kinase AKT, which is activated during BCR signalling. SGK, a related kinase (commonly mutated in this study), is known to phosphorylate FOXO3a in a similar way[7] and we predict it may also phosphorylate FOXO1. Thus, mutations affecting the FOXO1 phosphorylation site or SGK1 could affect the regulation of FOXO1 nuclear localization and hence, its transactivation activity. The shortened FOXO1 protein produced by mutation of the initial codon (Figure S2) would not contain this phosphorylation site and hence those mutations may also result in altered subcellular localization. Various mutations affecting NF-kB activity, which have been previously described, were also observed here[8,9,10,11]. (D) Many of the recurrently mutated genes in B-NHL are involved in histone modification or themselves encode histone proteins (i.e. *HIST1H1C*, one of multiple genes that encode histone protein H1). CREBBP/EP300 and MLL2 each produce activating chromatin marks (H3K27Ac and H3K4me3, respectively). HDAC (e.g. HDAC7) and EZH2 produce inactivating marks by removing acetyl groups and trimethylating H3K27, respectively. As heterozygous *EZH2* Y641 mutations are known to effectively enhance PRC2 activity[12], then each of the individual mutations may result in suppression of gene expression. Importantly, it is not known whether EZH2 and MLL2 regulate the expression of the same genes as MEF2B/CREBBP/EP300.

A

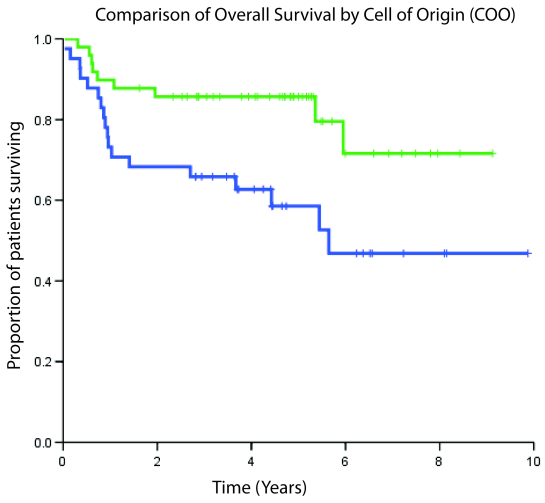
Comparison of Overall Survival by Cell of Origin (COO)
Proportion of patients surviving
1.0
0.8
0.6
0.4
0.2
0.0
0
2
4
6
8
10
Time (Years)

B

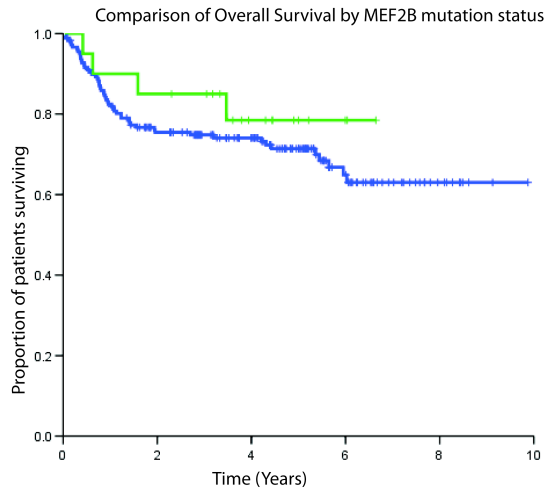
Comparison of Overall Survival by MEF2B mutation status
Proportion of patients surviving
1.0
0.8
0.6
0.4
0.2
0.0
0
2
4
6
8
10
Time (Years)

C

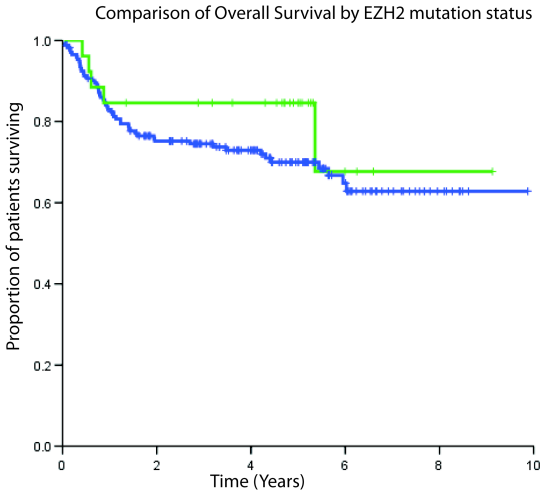
Comparison of Overall Survival by EZH2 mutation status
Proportion of patients surviving
1.0
0.8
0.6
0.4
0.2
0.0
0
2
4
6
8
10
Time (Years)

Figure S6: No detectable prognostic impact of EZH2 or MEF2B mutations in DLBCL.
The presence of MEF2B mutations (in exon 1 or 2) and EZH2 hot spot (Y641) mutations was determined in a cohort of 199 DLBCL patients, the subset of the 259 DLBCL cases that were uniformly treated with R-CHOP. (A) The overall survival times (OS) were compared between the uniformly treated patients in this cohort for the cases with known COO subtype, as defined by gene expression profiling (GEP)[13](Methods). The GCB cases (green, n=49) showed superior OS when compared to the ABC cases (blue, n=41)(P=0.012, Log-rank test). (B) Cases found to have mutations in MEF2B (green) were compared to those lacking mutations (blue) and no significant difference in OS was found (p = 0.399, Log-rank test). (C) Analysis of DLBCL patients with (green) and without (blue) mutations affecting Y641 in EZH2 also showed no significant difference (p = 0.279, Log-rank test). Hence, although these mutations appear to be strongly enriched in GCB cases, they do not appear enriched among cases with particularly good (or poor) outcomes.

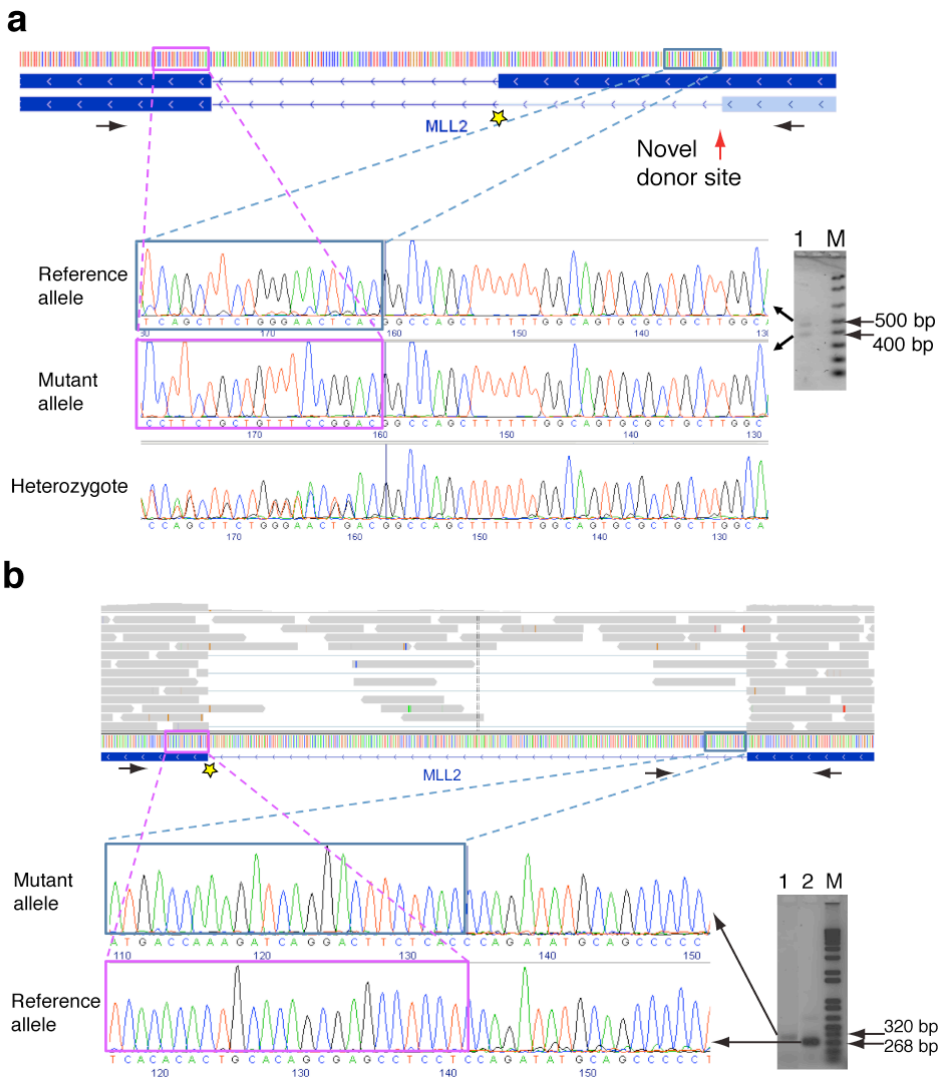

Figure S7: Confirmation of alternative splicing events resulting from MLL2 splice site mutations.

Shown are two examples of the effect of somatic splice site mutations in the MLL2 gene (reverse strand) determined from RNA-seq data and verified by Sanger sequencing (Supplementary Table S10; 05-25439).(A) Point mutation affecting a splice donor site (GT>GA) at chr12:47,714,115 (yellow star). RT-PCR primers for exons 38 and 39 (blue rectangles) are indicated by black arrows. Sequence from the upper gel band represents the reference allele or, from the lower band, the alternative transcript which uses an alternative donor site within exon 38. (B) Point mutation that disrupts a splice acceptor site (AG>CG) at chr12:47,733,692 (yellow star). Intron retention is inferred due to enrichment of intronic sequence reads (top, grey bars). Black arrows depict PCR primers. Primers for exons 5 and 6 (lane 2 of gel on right) produced an amplicon of 267bp and an amplicon of 602bp. The difference in these sizes is the size of the intron (335bp). Primers for exon 5 and the intron (lane 1) produced a single amplicon of 318bp. Amplicon sequencing confirmed the present of the reference splicing pattern and the intron retention event.

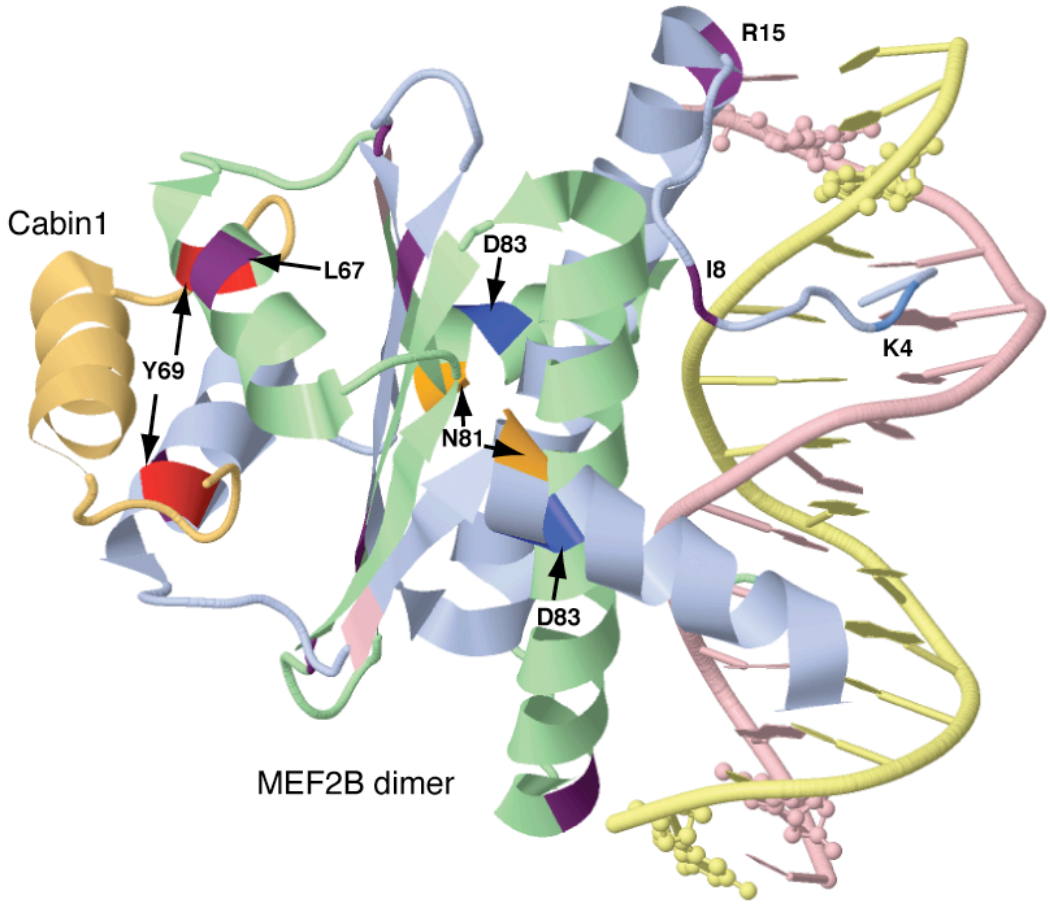

Figure S8: Visualization of MEF2B mutations in the solved crystal structure.
The crystal structure of MEF2B bound to one of its co-repressors (Cabin1) is shown with the mutated residues indicated[14]. Some of the mutations affect regions of the protein that interact with co-activators and co-repressors (e.g. Y69, L67) and regions that are likely to interact with DNA (e.g. K4). The crystal structure of MEF2A bound to EP300 has also recently been solved and supports that L67 and Y69 are also important in that interaction[15].

Supplementary Tables

Table S3: Gene fusions identified using RNA-seq and genome sequencing

Patient	Gene fusion(s)	Observed in*	Origin	Breakpoint 1	Breakpoint 2
DLBCL-Patient C	*KIAA1532/ POLR2E*	Transcriptome only	Unknown	chr19:2254040	chr19:1040471
DLBCL-Patient D	*BCL2/ IGH*	Both	Somatic	chr18:58944471	chr14:105401497
	C15orf57/ CBX3	Both	Germ line**	chr15:38641486	chr7:26219496
DLBCL-Patient E	None	NA	NA	NA	NA
DLBCL-Patient F	None	NA	NA	NA	NA
DLBCL-Patient G	*BCL2/ IGH*	Both	Somatic	chr18:58945022	chr14:105453733
DLBCL-Patient H	*MAPKBP1 /MGA*	Both	Germ line	chr15:39837967	chr15:39903511
	SMEK1/ CCDC88C	Both	Germ line	chr14:90867139	chr14:91005988
DLBCL-PatientI	None	NA	NA	NA	NA
DLBCL-Patient J	*IGH/ DUSP22*	Both	Somatic	chr14:105396245	chr6:295806
DLBCL-Patient K	*C15orf57/ CBX3*	Both	Germ line**	chr15:38641486	chr7:26219496
	GIT1/ SHMT1	Both	Somatic	chr17:18177820	chr17:24935050
	YES1/ ENOSF1	Transcriptome only	Unknown	chr18:714633	chr18:696468
DLBCL-Patient L	*BCL2/ IGH*	Both	Somatic	chr18:58915791	chr14:105400505
DLBCL-Patient M	*BCL6/ FBX018*	Both	Somatic	chr3:188945185	chr10:6018457
	C15orf57/ CBX3	Both	Germ line**	chr15:38641486	chr7:26219496
	C4orf18/ TMEM144	Both	Germ line	chr4:159303043	chr4:159380815

*Events observed only in the transcriptome are potential false positive events or the result of trans-splicing;**Genome sequencing reveals that this germ line derived event is not the result of a genomic translocation but rather the approximately 7 Kb insertion of chr7 sequence (harbouring *CBX3*) into the chr15 region containing *C15orf57*.

Table S6: Mutation hotspots in genes identified using RNA-seq.

Codon	Number of Samples	Distinct mutations	Gene Name
602;646	30	4	***EZH2***
83§	9	2	*MEF2B*
69§	4	2	*MEF2B*
81§	2	2	*MEF2B*
1482§	3	2	*CREBBP*
1499§	2	2	*CREBBP*
1467§	2	2	*EP300*
287§	2	1	*HLA-C*
1	8	5	***BCL7A‡***
206§	4	1	***MYD88‡***
230§	2	1	***MYD88‡***
252§	6	1	***MYD88‡***
59	7	3	***BCL2****
92;196;197	5	4	***CD79B‡***
73;160§	4	2	*IKZF3‡*
164;255§	3	2	***PIM1‡***
97;188	3	2	***PIM1‡***
18§	3	2	***IRF4‡***
587§	3	2	***BCL6***
45§	3	2	*BTG2‡*
141;234	3	2	***TP53‡***
24§	2	2	*FOXO1‡*
1§	3	3	*FOXO1‡*
12§	2	1	***TNFRSF14***
226§	2	2	*CCND3‡*
233§	2	2	*CCND3‡*
1§	3	3	*B2M‡*

§This mutation was proven to be somatic in at least one case; that is, present in tumour DNA but absent in matched constitutional DNA. ‡Not mutated in any of the fourteen genomes or exomes sequenced. *Additional hot spots in BCL2 were excluded to simplify the table. Genes indicated in bold are previously described targets of somatic mutation in lymphoma. Although known to be mutated, hot spots have not, to our knowledge, been described in *BCL7A*. Note that Tyr641 as previously described[16] is based on the Uniprot sequence Q15910, whereas this site corresponds to residue 602 and 646 in the Refseq annotations.

Table S9: Mutations affecting *CREBBP* or *EP300* detected using RNA-seq data.

Library	Disease	Gene	Annotation	*EP300* position
HS0841	DLBCL line	*CREBBP*	E1238*;E1268*	E1202
HS0842	DLBCL line	*CREBBP*	A436V	A420
HS0842	DLBCL line	*CREBBP*	Q170*;Q238*	not conserved
HS0806	FL	*CREBBP*	Y71H;Y1482H;Y1512H§	Y1446
HS1185	FL	*CREBBP*	G1411E;G1441E	**G1375**
HS1200	FL	*CREBBP*	Y92F;Y1503F;Y1533F	**Y1467**
HS1360	FL	*CREBBP*	R35C;R1446C;R1476C	**R1410**
HS1361	FL	*CREBBP*	S25N;S1436N;S1466N§	S1400
HS0637	DLBCL	*CREBBP*	Q1104*;Q1134*	Q1068
HS0641	DLBCL	*CREBBP*	L88Q;L1499Q;L1529Q§	L1463
HS0649	DLBCL	*CREBBP*	P77R;P1488R;P1518R§	P1452
HS0649	DLBCL	*CREBBP*	A687V;A717V	not conserved
HS0749	DLBCL	*CREBBP*	N1589K;N1619K	N1552
HS0933	DLBCL	*CREBBP*	R370*;R438*	R354
HS0939	DLBCL	*CREBBP*	M1625V;M1655V§	M1588
HS1135	DLBCL	*CREBBP*	V1342E;V1372E	V1306
HS1460	DLBCL	*CREBBP*	L88P;L1499P;L1529P§	L1463
HS1977	DLBCL	*CREBBP*	C1283R;C1313R	C1247
HS1979	DLBCL	*CREBBP*	N513S;N1978S;N2008S	not conserved
HS2059	DLBCL	*CREBBP*	Y71N;Y1482N;Y1512N§	Y1446
HS2249	DLBCL	*CREBBP*	A442T;A1907T;A1937T	not conserved
HS2249	DLBCL	*CREBBP*	Y92H;Y1503H;Y1533H§	**Y1467**
HS2606	DLBCL	*CREBBP*	R35C;R1446C;R1476C§	**R1410**
HS0653	DLBCL	*EP300*	Q1904*	-
HS0939	DLBCL	*EP300*	A1498T§	-
HS1133	DLBCL	*EP300*	L415P	-
HS1462	DLBCL	*EP300*	**Y1467H**§	-
HS2049	DLBCL	*EP300*	P925T‡	-
HS2607	DLBCL	*EP300*	P925T‡	-
HS1199	FL	*EP300*	D1485V	-
HS1201	FL	*EP300*	Q1455L	-
HS1202	FL	*EP300*	**Y1467N**§	-
HS0841	DLBCL line	*EP300*	Q160*	-
HS0900	DLBCL line	*EP300*	R1627W	-

§mutation was proven to be somatic (absent in matched constitutional DNA); ‡was also found in the matched constitutional DNA (inherited variant); bold indicates mutation hot spots.

Table S11: All *MEF2B* mutations detected.

Case (res_id)	Position (chromosome)	Change (DNA)	Change (protein)	Diagnosis and subtype (subtyping method)
03-31934	chr19:19122543	T > A	M1K	FL
02-17440	chr19:19122535	A > G	K4E	GCB DLBCL (GEP)
98-17403	chr19:19122535	A > G	K4E	DLBCL
06-20044	chr19:19122535§	A > G	K4E	FL
06-23741	chr19:19122535§	A > G	K4E	FL
07-14540	chr19:19122535	A > G	K4E	FL
98-14740	chr19:19122535	A > G	K4E	FL
05-15463	chr19:19122532	A > G	K5E	FL
03-28045	chr19:19122523	A > G	I8V	DLBCL
92-59893	chr19:19122502	A > G	R15G	DLBCL
02-28712	chr19:19122492	C > T	Q18*	DLBCL
05-22052	chr19:19121225	A > G	K23R	DLBCL
07-10201	chr19:19121222	G > A	R24Q	FL
SPEC1187	chr19:19121217	T > G	F26V	GCB DLBCL (GEP)
06-20952	chr19:19121195	A > C	Y33S	FL
03-18669	chr19:19121153	T > C	I47T	DLBCL
03-33888	chr19:19121135	G > A	R53H	DLBCL
01-16433	chr19:19121093§	T > G	L67R	FL
00-15694	chr19:19121088§	A > G	Y69H	GCB DLBCL (GEP)
05-11328	chr19:19121088	A > G	Y69H	GCB DLBCL (GEP)
06-12968	chr19:19121087§	T > C	Y69C	FL
06-18193	chr19:19121087	T > C	Y69C	FL
08-10448	chr19:19121087	T > C	Y69C	FL
99-30068	chr19:19121087	T > C	Y69C	FL
05-11369	chr19:19121066	-GGGGCT	E74-P75-H76 > D	FL
06-23851	chr19:19121066	A > G	H76R	FL
07-21828	chr19:19121064	G > A	E77K	DLBCL
07-30109	chr19:19121063	A > G	E77G	Composite FL
06-30145	chr19:19121052§	A > T	N81Y	GCB DLBCL (GEP)
05-23110	chr19:19121050§	C > A	N81K	GCB DLBCL (GEP)
00-13940	chr19:19121045	T > G	D83A	GCB DLBCL (IHC)
06-15922	chr19:19121045§	T > G	D83A	GCB DLBCL (GEP)
07-23804	chr19:19121045	T > G	D83A	GCB DLBCL (GEP)
00-22287	chr19:19121045	T > A	D83V	GCB DLBCL (IHC)
01-18672	chr19:19121045	T > A	D83V	GCB DLBCL (IHC)
02-30647	chr19:19121045§	T > A	D83V	GCB DLBCL (GEP)
03-11110	chr19:19121045	T > A	D83V	DLBCL
03-26817	chr19:19121045	T > A	D83V	GCB DLBCL (GEP)
03-30438	chr19:19121045	T > A	D83V	GCB DLBCL (GEP)
05-24666	chr19:19121045	T > A	D83V	GCB DLBCL (GEP)
06-30025	chr19:19121045§	T > A	D83V	GCB DLBCL (GEP)

06-33777	chr19:19121045§	T > A	D83V	GCB DLBCL (GEP)
78-60284	chr19:19121045	T > A	D83V	GCB DLBCL (IHC)
95-32814	chr19:19121045§	T > A	D83V	GCB DLBCL (GEP)
97-10270	chr19:19121045	T > A	D83V	DLBCL
DB (cell line)	chr19:19121045	T > A	D83V	GCB DLBCL (GEP)
06-11109	chr19:19121045	T > G	D83A	FL
07-20462	chr19:19121045	T > G	D83A	FL
91-34915	chr19:19121045	T > G	D83A	FL
03-16286	chr19:19121045	T > C	D83G	FL
05-12024	chr19:19121045	T > A	D83V	FL
06-22766	chr19:19121045	T > A	D83V	FL
06-33903	chr19:19121045	T > A	D83V	FL
89-30159	chr19:19121045	T > A	D83V	FL
91-53679	chr19:19121045	T > A	D83V	FL
97-23234	chr19:19121045	T > A	D83V	FL
99-21548	chr19:19121045	T > A	D83V	FL
01-24821	chr19:19119600	+A	L100 Frameshift	FL
85-31959	chr19:19119578	C > A	E108*	FL
06-16716	chr19:19119559‡	C > T	R114Q	ABC DLBCL (GEP)
02-18484	chr19:19119539	10bp del	G121 Frameshift	FL
91-53679	chr19:19118877	-GGAA	F170 Frameshift	FL
08-15460	chr19:19118875	-AAGG	P169 Frameshift	DLBCL
06-10398	chr19:19118406	+GG	G242 Frameshift	ABC DLBCL (GEP)
06-30389	chr19:19118365	-C	P256 Frameshift	FL
07-18609	chr19:19117831	A > C	S294R†	FL
05-20543	chr19:19117794	G > T	R307S†	ABC DLBCL (GEP)
05-14545	chr19:19117608	A > G	*369G†	FL
06-23851	chr19:19117608	A > C	*369E†	FL
06-12557	chr19:19117606	C > G	*369Y†	FL

†annotation is unique to NM_001145785, representing the longest MEF2B isoform; §was proven to be somatic (absent in matched constitutional DNA); ‡was also found in the matched constitutional DNA (inherited variant)

Table S12: Catalogue of *MEF2B* cSNVs in FL and DLBCL.

Amino Acid Change	FL	DLBCL	Total	% variants
M1K	1	0	1	1.4
K4E[§]	4	2	6	8.7
K5E	1	0	1	1.4
I8V	0	1	1	1.4
R15G	0	1	1	1.4
K23R	0	1	1	1.4
R24Q	1	0	1	1.4
F26V	0	1	1	1.4
Y33S	1	0	1	1.4
I47T	0	1	1	1.4
R53H	0	1	1	1.4
L67R	1	0	1	1.4
Y69C/H[§]	4	2	6	8.7
E74-P75-H76 > D	1	0	1	1.4
H76R	1	0	1	1.4
E77K	0	1	1	1.4
N81K/Y[§]	0	2	2	2.9
D83A/G/V[§]	11	16	27	39.1
R114Q	0	1	1	1.4
S294Y	1	0	1	1.4
R307S	0	1	1	1.4
*369Y/E/G	3	0	3	4.3
Truncation	5	3	8	11.6
Any mutation	35	34	69	100.0
Total cases sequenced	261	292		
Prevalence	13.41%	11.64%		

[§]at least one representative mutation at this position has been confirmed as a somatic mutation.

Supplementary Discussion

It is thought that GCB and ABC DLBCLs arise due to distinct genetic events[17] and it is widely accepted that the aggressive nature of the latter results from the acquisition of mutations that mimic stimulation of the B cell receptor by antigen or those that more directly induce constitutive activation of NF-kB[18]. Here we report other important modulators or components of BCR signalling and regulators of B cell differentiation or survival as targets of repeated and recurrent mutation, including *MEF2B/C*[5], *SGK1*[7], *IRF4*[19], *STAT3*[3], *STAT6*[20], *RFTN1*[21], *CCND3*[22], *PLCG2*, *FOXO1*[23], *CARD11*[8], *CD79B*[9] and *MYD88*[10] and *IKZF3*[24]. There were notable differences in mutation patterns among these genes. For example, *MEF2B/C* and *STAT3*, each of which function as dimers, showed strong evidence for selectively acquiring nonsynonymous (rather than truncating) mutations, whereas *SGK1* and *CCND3* appeared to be preferentially truncated in NHL. The previously characterized *CARD11*[8], *CD79B*[9] and *MYD88*[10] all act upstream of NF-kB, leading to its deregulation, typically in ABC DLBCLs. In our data, only *CD79B* and *MYD88* (in addition to structural rearrangements involving *BCL6*) showed a significant enrichment for mutations in ABC cases (Figure 2) and the point mutations we observed largely corresponded to the known hot spots in these two genes[9,10](Table S6).

The remaining genes listed above encode proteins that are either activated or inhibited as a result of BCR stimulation, but not directly involved in regulating NF-kB. *PRDM1* has been termed the plasma cell master differentiation gene as it orchestrates terminal differentiation of germinal centre B cells into plasma cells[25].

Importantly STAT3[3], found here to be commonly mutated in DLBCL, regulates the activity or expression of *PRDM1* in response to IL-21 stimulation. Of interest, inherited mutations in *STAT3* are the primary cause of an immune disorder known as hyper IgE syndrome and it has been shown that in these cases mutant STAT3 acts in a dominant negative manner[26]. Strikingly, some of the somatic mutations we report here affect the same residues found mutated in the constitutional DNA of hyper IgE patients. This leads us to predict that mutant cells may be unable to induce *PRDM1* transcription following IL-21 stimulation (Figure S5A). In particular, as many of these mutations were found in both GCB DLBCL and FL, our data suggest that malignant transformation of germinal centre B cells relies on components of BCR signalling separate from those utilized in ABC DLBCL (i.e. NF-kB) but also that altered regulation of *PRDM1*, previously thought to be a feature unique to ABC DLBCL, may be of general importance in NHL.

Mutations affecting *CREBBP* and *EP300* were recently reported in DLBCL[27], and ALL[28]. Similar to the observations reported in these studies, our data show a preference for accumulation of truncating SNVs (n=4, 16.7% of mutated cases) but also include non-synonymous SNVs in many cases (20 cases with cSNVs, Table S9). *EP300* also contained multiple cSNVs (8 cases total). We confirmed that 3 *EP300* cSNVs and 9 *CREBBP* cSNVs were somatic mutations. Cases with multiple cSNVs in either gene were rarely observed (one cell line and three patients) consistent with the commonly held notion that both genes are haploinsufficient[29]. The cSNVs that were not predicted to result in protein truncation were mainly found within the HAT domain of these two

proteins. These included four codons that are apparent mutation hot spots (Tables S6 and S9). Of these, three correspond to residues that have been reported to be homologous between the two proteins[1] (Figure S3; Table S9). Representative cSNVs corresponding to three of these hot spots in *CREBBP* and one in *EP300* were confirmed as somatic. Three of the *EP300* somatic non-synonymous mutations we observed affected residues previously shown to reduce acetyltransferase activity in an *in vitro* acetyltransferase assay (Figure S3)[1]. We also confirmed that *CREBBP* (but not *EP300*) has a significant signature of selective pressure to acquire both truncating and missense mutations (Table 1), but the lack of significance for the latter may owe to limited statistical power due to its reduced mutation prevalence relative to *CREBBP*. Taken together, these data suggest that reduction or loss of either *CREBBP* or *EP300* may promote lymphomagenesis. Of note, in contrast to a recent report[27], we did not observe a significant difference in *CREBBP* or *EP300* mutation frequency in the two subtypes (P = 0.5656 for *CREBBP* and 0.6607 for *EP300*; Fisher exact test).

MEF2 proteins can act as transcriptional co-activators or co-repressors by recruiting two classes of enzymes that alter the acetylation state of histone tails, namely HATs and HDACs. MEF2 dimers are known to associate with the two HATs CREBBP and EP300[30] and it has been suggested that HDACs and CREBBP/EP300 compete for the same binding site on MEF2[31]. Under normal levels of intracellular Ca^{2+}, MEF2 is bound by one of several type IIa HDACs, which maintain the tails of histone proteins in a deacetylated repressive chromatin state[32]. Increased cytoplasmic Ca^{2+} levels induce the nuclear export of the bound HDAC, thus enabling MEF2 dimers to recruit a HAT enzyme such

as CREBBP/EP300, which facilitate transcription at MEF2 target genes by catalysing the addition of acetyl groups to the tails of core histone proteins including lysine 27 on histone H3 (H3K27)[30,31](Figure S5D).

Ca^{2+}-mediated induction of MEF2 target genes is utilised in diverse developmental processes including muscle and neuronal cell differentiation[33] as well as the maturation of B and T cells[6]. For example, during negative selection, upon T-cell-receptor (TCR) stimulation, the resulting Ca^{2+} influx results in MEF2-mediated induction of the pro-apoptosis *NR4A1* (NUR77), which, in turn drives apoptosis of self-reactive T cells[6]. It has also been shown in T cells that MEF2D interacts directly with nuclear NFAT, another Ca^{2+}/CaM-regulated protein, and recruits EP300 to MEF2 target genes[34]. In murine B cells, it was recently demonstrated that MEF2C is required to mediate gene expression events following BCR stimulation, but this study did not discuss a possible overlapping role of MEF2B in this process nor was there a conclusive identification of the MEF2C-regulated genes important to this process[5]. That we also observed mutations in *MEF2C* at a lower frequency in NHL samples supports the interpretation that these proteins share a related function in this cellular context. The MEF2B dimer has previously been co-crystallized with three of its interacting partners, namely Cabin1[14], HDAC9[31] and EP300[15] and, informed by these structures, we predict that many of the recurrent mutations would negatively impact the function of MEF2B. For example, at least three of the mutated residues (K5, K23 and R24) are required for mediating the binding of MEF2 to DNA[35]. Because MEF2 proteins can heterodimerize[36], mutations that impact the

function of MEF2 are known to produce a dominant effect on the overall function of any MEF2-family protein by occupying a significant proportion of MEF2-containing complexes[37]. In fact one of the residues found mutated in this study (K24) was previously demonstrated to act as a dominant negative when ectopically expressed[37]. Further, we also note that the mutation hot spot Y69 was recently shown to be involved in multiple interactions in a solved crystal structure of MEF2B bound to EP300[15], suggesting the possibility that this mutation may impact the ability of these two proteins to interact. Although the impact of the individual *MEF2B* mutations on MEF2 function requires further study, the recurrence of these mutations among a limited set of residues suggests the action of positive selection for these mutations during cancer progression.

When one considers the high frequency of mutations we detected that affect genes encoding MEF2 proteins, it is striking but perhaps not surprising that inactivating mutations affecting both CREBBP and EP300 are common in NHL, as these are both known effectors of the induction of MEF2-regulated genes. Notably, with one exception, all of the truncation-inducing mutations identified in *CREBBP* and *EP300* are predicted to remove the histone acetyltransferase (HAT) domain of the protein[14]. Moreover, comparison of the positions mutated in *CREBBP* to those mutated in *EP300* reveals that some homologous residues within the HAT domains are affected in both proteins (Figure S3). Based on the crystal structure of EP300, five of these recurrently mutated residues were previously identified as important for mediating substrate interaction[1]. In that

study, three of these residues were mutated and showed loss (or reduction) of HAT activity *in vitro,* suggesting that many of the cSNVs we observed in these two proteins also negatively impact their function *in vivo*. Further, CREBBP/EP300 are both known to regulate the function of FOXO1[38], another gene found recurrently mutated in this study. Thus it is also possible that the mutation of these genes in addition their potential effect on MEF2-mediated transactivation, could impact the normal AKT-mediated nuclear exclusion of FOXO1 (Figure S5C).

Our data are consistent with a model wherein the induction of MEF2 target genes in response to BCR stimulation is inhibited by mutations that reduce the function of MEF2 complexes, potentially in a dominant negative fashion, or mutations that inactivate either of their transcriptional co-activators CREBBP or EP300 (Figure S5D). Another mutation identified in this study in a single case is also consistent with our model, namely the mutation of S155 to phenylalanine in *HDAC7*. This serine residue is known to be phosphorylated by CAMK following TCR stimulation, facilitating nuclear export of HDAC7 in response to Ca^{2+} influx[39]. In the cited study, mutation of this residue resulted in impaired export of HDAC7 following TCR stimulation thereby inhibiting MEF2-mediated induction of NUR77 expression and hence, inhibiting NUR77-mediated apoptosis. Thus, this mutant could potentially produce a nuclear-restricted protein that leads to constitutive suppression of MEF2 target genes regardless of intracellular Ca^{2+} levels. This would be a similar effect that would be expected for loss-of-function mutations of *MEF2B*, *CREBBP* or *EP300*. Though an increase in cytoplasmic Ca^{2+} is one

downstream signal following BCR stimulation, the NFAT transcription factors, key downstream mediators of this signal that promote survival, were not mutated and thus are expected to function normally. Also, pathways such as NF-kB and events modulated by AKT do not rely on the Ca^{2+} messenger and should therefore be unaffected by these mutations. Interestingly, a recent report suggests that SGK1 (found here to be commonly inactivated in DLBCL) may also play a role in modulating Ca^{2+} levels by regulating the turnover of the Ca^{2+} channel protein Orai[40]. Thus, this model predicts that mutations directly affecting MEF2 function (i.e. those in *MEF2B, MEF2C*, *HDAC7*, *CREBBP* or *EP300*) or other genes involved in regulating cytoplasmic calcium levels would diminish the cell's ability to induce MEF2 target genes in response to BCR stimulation while leaving other downstream signals intact.

References

1. Liu, X. et al. The structural basis of protein acetylation by the p300/CBP transcriptional coactivator. *Nature* **451**, 846–850 (2008).
2. Lewis, B.P., Green, R.E. & Brenner, S.E. Evidence for the widespread coupling of alternative splicing and nonsense-mediated mRNA decay in humans. *Proc Natl Acad Sci USA* **100**, 189–192 (2003).
3. Diehl, S. et al. STAT3-mediated up-regulation of BLIMP1 Is coordinated with BCL6 down-regulation to control human plasma cell differentiation. *J Immunol* **180**, 4805–4815 (2008).
4. Ariel, O., Levi, Y. & Hollander, N. Signal transduction by CD58: The transmembrane isoform transmits signals outside lipid rafts independently of the GPI-anchored isoform. *Cell Signal* **21**, 1100–1108 (2009).
5. Wilker, P. et al. Transcription factor Mef2c is required for B cell proliferation and survival after antigen receptor stimulation. *Nat Immunol* **9**, 603–612 (2008).
6. Youn, H., Sun, L., Prywes, R. & Liu, J. Apoptosis of T cells mediated by Ca2+-induced release of the transcription factor MEF2. *Science* **286**, 790–793 (1999).
7. Brunet, A. et al. Protein Kinase SGK Mediates Survival Signals by Phosphorylating the Forkhead Transcription Factor FKHRL1 (FOXO3a). *Mol Cell Biol* **21**, 952–965 (2001).
8. Lenz, G. et al. Oncogenic CARD11 mutations in human diffuse large B cell lymphoma. *Science* **319**, 1676–1679 (2008).
9. Davis, R.E. et al. Chronic active B-cell-receptor signalling in diffuse large B-cell lymphoma. *Nature* **463**, 88–92 (2010).
10. Ngo, V.N. et al. Oncogenically active MYD88 mutations in human lymphoma. *Nature* **470**, 115–119 (2011).
11. Du, M.Q. et al. BCL10 gene mutation in lymphoma. *Blood* **95**, 3885–3890 (2000).
12. Yap, D.B. et al. Somatic mutations at EZH2 Y641 act dominantly through a mechanism of selectively altered PRC2 catalytic activity, to increase H3K27 trimethylation. *Blood* **117**, 2451–2459 (2011).
13. Wright, G. et al. A gene expression-based method to diagnose clinically distinct subgroups of diffuse large B cell lymphoma. *Proc Natl Acad Sci USA* **100**, 9991–9996 (2003).
14. Han, A. et al. Sequence-specific recruitment of transcriptional co-repressor Cabin1 by myocyte enhancer factor-2. *Nature* **422**, 730–734 (2003).
15. He, J. et al. Structure of p300 bound to MEF2 on DNA reveals a mechanism of enhanceosome assembly. *Nucleic Acids Res* (2011).doi:10.1093/nar/gkr030
16. Morin, R.D. et al. Somatic mutations altering EZH2 (Tyr641) in follicular and diffuse large B-cell lymphomas of germinal-center origin. *Nat Genet* **42**, 181–185 (2010).
17. Lenz, G. et al. Molecular subtypes of diffuse large B-cell lymphoma arise

by distinct genetic pathways. *Proc Natl Acad Sci USA* **105**, 13520–13525 (2008).
18. Lenz, G. & Staudt, L.M. Aggressive lymphomas. *N Engl J Med* **362**, 1417–1429 (2010).
19. Hunt, K.E., Hall, B. & Reichard, K.K. Translocations involving MUM1 are rare in diffuse large B-cell lymphoma. *Appl Immunohistochem Mol Morphol* **18**, 109–112 (2010).
20. Linehan, L.A., Warren, W.D., Thompson, P.A., Grusby, M.J. & Berton, M.T. STAT6 is required for IL-4-induced germline Ig gene transcription and switch recombination. *J Immunol* **161**, 302–310 (1998).
21. Saeki, K., Miura, Y., Aki, D., Kurosaki, T. & Yoshimura, A. The B cell-specific major raft protein, Raftlin, is necessary for the integrity of lipid raft and BCR signal transduction. *EMBO J* **22**, 3015–3026 (2003).
22. Peled, J.U. et al. Requirement for cyclin D3 in germinal center formation and function. *Cell Res* **20**, 631–646 (2010).
23. Srinivasan, L. et al. PI3 kinase signals BCR-dependent mature B cell survival. *Cell* **139**, 573–586 (2009).
24. Cortés, M. & Georgopoulos, K. Aiolos is required for the generation of high affinity bone marrow plasma cells responsible for long-term immunity. *J Exp Med* **199**, 209–219 (2004).
25. Shaffer, A.L. et al. Blimp-1 orchestrates plasma cell differentiation by extinguishing the mature B cell gene expression program. *Immunity* **17**, 51–62 (2002).
26. Minegishi, Y. et al. Dominant-negative mutations in the DNA-binding domain of STAT3 cause hyper-IgE syndrome. *Nature* **448**, 1058–1062 (2007).
27. Pasqualucci, L. et al. Inactivating mutations of acetyltransferase genes in B-cell lymphoma. *Nature* **471**, 189–195 (2011).
28. Mullighan, C.G. et al. CREBBP mutations in relapsed acute lymphoblastic leukaemia. *Nature* **471**, 235–239 (2011).
29. Janknecht, R. The versatile functions of the transcriptional coactivators p300 and CBP and their roles in disease. *Histol. Histopathol* **17**, 657–668 (2002).
30. Giordano, A. & Avantaggiati, M. p300 and CBP: partners for life and death. *J Cell Physiol* **181**, 218–230 (1999).
31. Han, A., He, J., Wu, Y., Liu, J.O. & Chen, L. Mechanism of recruitment of class II histone deacetylases by myocyte enhancer factor-2. *J Mol Biol* **345**, 91–102 (2005).
32. Youn, H. & Liu, J. Cabin1 represses MEF2-dependent Nur77 expression and T cell apoptosis by controlling association of histone deacetylases and acetylases with MEF2. *Immunity* **13**, 85–94 (2000).
33. Potthoff, M. & Olson, E. MEF2: a central regulator of diverse developmental programs. *Development* **134**, 4131–4140 (2007).
34. Youn, H.D., Chatila, T.A. & Liu, J.O. Integration of calcineurin and MEF2 signals by the coactivator p300 during T-cell apoptosis. *EMBO J* **19**, 4323–4331 (2000).

35. Wu, W. et al. Conservation and evolution in and among SRF- and MEF2-type MADS domains and their binding sites. *Molecular biology and evolution* (2010).doi:10.1093/molbev/msq214
36. Martin, J. et al. A Mef2 gene that generates a muscle-specific isoform via alternative mRNA splicing. *Mol Cell Biol* **14**, 1647–1656 (1994).
37. Molkentin, J.D., Black, B.L., Martin, J.F. & Olson, E.N. Mutational analysis of the DNA binding, dimerization, and transcriptional activation domains of MEF2C. *Mol Cell Biol* **16**, 2627–2636 (1996).
38. van der Heide, L.P. & Smidt, M.P. Regulation of FoxO activity by CBP/p300-mediated acetylation. *Trends Biochem. Sci.* **30**, 81–86 (2005).
39. Dequiedt, F. et al. HDAC7, a thymus-specific class II histone deacetylase, regulates Nur77 transcription and TCR-mediated apoptosis. *Immunity* **18**, 687–698 (2003).
40. Eylenstein, A. et al. Stimulation of Ca2+-channel Orai1/STIM1 by serum- and glucocorticoid-inducible kinase 1 (SGK1). *FASEB J* **25**, 2012–2021 (2011).